



## Flexural-Torsional Galloping of Prismatic Structures with Double-Symmetric Cross-Section

Angelo Luongo<sup>1</sup>, Francesca Pancella<sup>2</sup>, Giuseppe Piccardo<sup>3</sup>

<sup>1</sup>M&MoCS - University of L'Aquila, Loc. Monteluco di Roio, 67100 L'Aquila, AQ, Italy, Email: angelo.luongo@univaq.it

<sup>2</sup>M&MoCS - University of L'Aquila, Loc. Monteluco di Roio, 67100 L'Aquila, AQ, Italy, Email: francesca.pancella@graduate.univaq.it

<sup>3</sup>DICCA - University of Genoa, Via Montallegro 1, 16145 Genova, GE, Italy, Email: giuseppe.piccardo@unige.it

Received September 28 2020; Revised November 15 2020; Accepted for publication November 16 2020.

Corresponding author: Giuseppe Piccardo (giuseppe.piccardo@unige.it)

© 2021 Published by Shahid Chamran University of Ahvaz

**Abstract.** The linear galloping of prismatic structures having double-symmetric cross-section, subjected to steady wind flow acting along a symmetry axis, is investigated. The continuous system is reduced to a three degree-of-freedom system via a Galerkin approach. The quasi-steady assumption for the aerodynamic forces is applied, under the hypothesis that the galloping instability is well-separated from the vortex induced vibration phenomenon. Due to the structural symmetry conditions and accounting for the aerodynamic coupling, galloping is of flexural-torsional type, occurring in the direction orthogonal to the incident wind. Moreover, coupling is stronger close to the resonance between the flexural and torsional degrees of freedom. A linear stability diagram is built up in a two-parameter space, highlighting the role of coupling in modifying the critical wind velocity, and in producing a veering phenomenon between the two modes. The existence of points at which a double-Hopf bifurcation manifests itself is detected. Both exact and perturbation solutions are provided, these latter in the non-resonant and resonant cases, useful to throw light on the interactive mechanisms. The resonant perturbation solution permits to analytically investigate under which conditions coupling has a detrimental effect on galloping, which manifests at a wind velocity lower than the flexural and torsional critical velocities. Situations where coupling between modes leads to beneficial effect with respect to the Den Hartog's critical wind velocity are also highlighted. As an application, galloping of a family of multi-story tower buildings having a square cross-section is studied.

**Keywords:** Galloping, Flexural-torsional interaction, Perturbation Methods, Veering, Tower building.

### 1. Introduction

The aeroelastic instability in a quasi-steady regime (called "galloping") is a typical phenomenon of aerodynamic instability that occurs in slender structures with non-circular section. Concerning a system with a single degree-of-freedom (DOF), orthogonal to the direction of the incident wind, the instability onset is defined by the well-known Den Hartog criterion [1], which is also used from a technical point of view in codes and guidelines (e.g., [2]) in order to estimate the structural safety with regard to critical conditions of galloping. The validity of these evaluations is linked to the quasi-steady flow hypothesis (e.g., [3]), which allows to deduce the dynamics of the body starting from aerodynamic coefficients obtained from static tests in wind tunnel. From a physical point of view, this means that forces are determined only by the instantaneous position and instantaneous relative velocity field of the flow around the cylinder, and that any memory effect is negligible. Such a hypothesis may be satisfied only if the characteristic times of the velocity fluctuations in the wake of the cylinder are much smaller than the characteristic times of the cylinder's oscillating motion. This happens for sufficiently high values of the reduced speed  $U_r = U/fb$  (where  $U$  is the value of mean wind velocity,  $f$  the cylinder's oscillation frequency and  $b$  a reference size of the cylinder cross section, e.g., its diameter or side), for example greater than 20 (e.g., [4]) for a square section (with sharp edges) since in this case the vortex-induced oscillations (VIVs) occur for  $U_r \simeq 7 - 8$ . The quasi-steady theory is usually considered as wind loading model also to take into account the effects of the gust-excited vibrations on slender structures (e.g., [5, 6]). Although the galloping onset is governed by the simple, deterministic Den Hartog criterion, actually its value is affected by uncertainties related to structural and aerodynamic parameters [7]. Evaluations of critical galloping conditions are possible for a single torsional degree-of-freedom too (e.g., [4]), even if in these cases the quasi-steady assumption is somewhat forced and not always valid but can in some cases perform well, at least in terms of onset [8]. Nigol and Buchan [9] have conducted detailed studies on conductors with natural ice shapes showing that galloping of overhead lines is caused largely by the torsional mechanism. For particular structures, such as slender towers (e.g., [10]) and shallow cables in transmission lines (e.g., [11]), not only the assessment of galloping critical conditions but also the analysis of post-critical oscillations is fundamental.

Focusing on the galloping onset, the study of sectional models with more degrees of freedom has attracted the interest of researchers in order to investigate the possible modifications with respect to the classic Den Hartog case. To the best knowledge of the authors, the first study that highlighted a galloping coupled response between plunging and torsional vibrations is due to Slater [12], with reference to a structural angle section. In this context, Iwan and Blevins [13] present a model for two degree-of-freedom instability, where the galloping is investigated by using asymptotic techniques to generate approximate steady-state



solutions. Stability criteria of these solutions are also presented showing that they fall into two classes, depending on the ratio of the natural frequencies in torsion and plunge [4]. The first class of solution is valid when the two frequencies are not approximately equal or in the ratio of small integers. When the two natural frequencies are close to an integer multiple (i.e., internal resonance 1/3, 1, 3), the approximate analysis yields equations which must be solved numerically. In this latter case there is a strong interaction between plunge and torsional modes, which appears greatest when the two structural frequencies are nearly equal. Desai et al. [14], in addition to the bluff angle section, analyze the galloping flexural-torsional behavior of a square section. Instability conditions are studied by applying the classic Routh-Hurwitz criterion; a limit cycle analysis in internal resonance as well as non-resonance conditions is treated by employing an averaging method. The example of square prism section points out that, near the 1:1 internal resonance condition, galloping can be initiated below the value predicted by a purely plunge approach. Therefore, torsion seems to play a significant role and predictions based on a classic plunge theory can be erroneous in resonance conditions. Later papers related to two DOF (plunge and torsion) galloping are addressed to iced cable sections [15, 16, 17], to study the effect of inertial coupling between the degrees of freedom due to iced conductor's eccentricity, making the 1:1 internal resonance vibration not possible.

The two-degree-of-freedom translational galloping has been examined starting from Jones' paper [18], where the solution of the eigenvalue equation indicates that the coupled galloping criterion may be either more or less stringent than the Den Hartog's criterion. A formula defining the onset wind velocity for the bi-dimensional coupled galloping oscillations of tower buildings in perfect 1:1 internal resonance is presented in [19]. The influence of the along-wind response on the across-wind vibration is also discussed in [20] to study the large amplitude aeroelastic vibration of highway tubular poles, starting from a continuous model and accounting for wind shear effects and variable cross-section. Through a perturbation approach, an approximated analytical solution for the eigenvalue problem is determined in [21]. Differently from the expressions existing in literature, the proposed eigensolutions are valid in both quasi-resonant and non-resonant conditions and allow depiction of all the possible bifurcation mechanisms in the plane of the invariants of the aerodynamic damping matrix. Moreover, a closed form expression for the critical velocity is derived; it coincides with the exact solution in the resonant case and presents very good agreement with the numerical solutions in quasi-resonant conditions. In this way the critical velocities are compared with the Den Hartog velocity and the influence of the horizontal motion is thus fully evaluated. In this context galloping critical conditions on square cylinders with an arbitrary attitude in the wind flow are studied in [22], and the dependence of the critical behavior on the orientation of the principal structural axes of the cross-section is presented in [23].

Moving to three degree-of-freedom sectional models capable of considering the two translations in the section plane together with the torsion, Piccardo [24] proposed a general model whose linearization allows to study numerically the incipient instability due to coupled aeroelastic phenomena in the Laplace domain. Yu et al. [25] developed a three DOF model to describe the galloping of a multi-span, electrical transmission line having an asymmetrically iced cross-section; galloping initiation conditions are studied according to the classic Routh-Hurwitz criterion. A similar approach to galloping critical conditions is presented in [26, 27] whereas He and Macdonald [28] focus on obtaining a closed-form solution for the effective aerodynamic damping of the 3 DOF system with perfectly tuned natural frequencies in the three structural modes, also considering the influence of inertial coupling [29]. Very recently Lou et al. [30] propose an analytical stability criterion for 3-DOF galloping response of iced transmission lines by using the eigenvalue perturbation method. The aerodynamic stiffness matrix is included in the zero-order stiffness matrix and analytical expressions for the real parts of the eigenvalues are determined without explicitly considering the possible internal resonance conditions that can occur between the three structural modes.

In this paper a continuous model representing a prismatic structure excited by a quasi-steady flow is considered. Through a Galerkin approach the system is reduced to a discrete three-DOF model which is coupled only in the flexural-torsional directions thanks to the hypothesis of double symmetry of the cross-section. The problem, therefore, becomes formally equal to a two DOF (plunge-torsional) sectional model, whose damping matrix is full due to the presence of the fluid-structure interaction terms, and in which there are also terms of aerodynamic stiffness of torsional nature. In this case an analytical study of incipient galloping in resonance and quasi-resonance conditions is still lacking in the literature. On the other hand, internal resonance interactions between the structural modes may be able to remarkably modify the critical conditions linked to the classic Den Hartog condition, as noted on a square prism section in [14]. The aim of the present work is a detailed exact (Sect 3) and perturbation analysis (Sect 4) of the critical conditions around the 1:1 resonance studying the matching to quasi-resonance and non-resonance conditions. Furthermore, as stated above, the discrete model (Sect 2) is not necessarily a sectional model (typically used in wind tunnel experiments) but can be interpreted as the discretization of a continuous model of prismatic structure. In this regard, Sect 5 presents the study of critical conditions for a shear-torsional building having a square cross-section in order to apply the proposed theory to a real structure. Some relevant conclusions are drawn in the ending Sect 6.

## 2. Discrete model

A prismatic structure of axis  $z$ , having bi-symmetric cross-section in the  $(x, y)$ -plane, subjected to a steady and uniform wind flow  $U$ , acting along the symmetry  $x$ -axis, is considered. The continuous structure is reduced to a three degree-of-freedom model via the Galerkin approach, in which  $\mathbf{q} = (u(t), v(t), \vartheta(t))^T$  are the amplitudes of the trial functions, describing the along-wind, cross-wind and twist amplitudes, respectively, and  $t$  is the time. By applying the quasi-steady theory for the aerodynamic forces (e.g., [3]), which holds when galloping is well-separated by the vortex shedding synchronization phenomenon, the linearized equations of motion are:

$$\mathbf{M}\ddot{\mathbf{q}} + (\mathbf{C}_s + \mathbf{C}_a)\dot{\mathbf{q}} + (\mathbf{K}_s + \mathbf{K}_a)\mathbf{q} = \mathbf{0} \tag{1}$$

Here:

$$\mathbf{M} := \begin{pmatrix} M & 0 & 0 \\ 0 & M & 0 \\ 0 & 0 & \mathcal{J}_G \end{pmatrix}, \quad \mathbf{C}_s := \begin{pmatrix} 2\xi_x\sqrt{K_x M} & 0 & 0 \\ 0 & 2\xi_y\sqrt{K_y M} & 0 \\ 0 & 0 & 2\xi_\vartheta\sqrt{K_\vartheta M} \end{pmatrix}, \quad \mathbf{K}_s := \begin{pmatrix} K_x & 0 & 0 \\ 0 & K_y & 0 \\ 0 & 0 & K_\vartheta \end{pmatrix} \tag{2}$$

$$\mathbf{C}_a := \frac{1}{2}\rho_a U b L \begin{pmatrix} 2c_d & 0 & 0 \\ 0 & (c_d + c'_l) & -R(c_d + c'_l) \\ 0 & bc'_m & -Rbc'_m \end{pmatrix}, \quad \mathbf{K}_a := \frac{1}{2}\rho_a U^2 b L \begin{pmatrix} 0 & 0 & 0 \\ 0 & 0 & c'_l \\ 0 & 0 & bc'_m \end{pmatrix}$$

are, in the order: the inertia matrix, the structural damping matrix, the structural stiffness matrix, the aerodynamic damping matrix, the aerodynamic stiffness matrix. Moreover:  $M, \mathcal{J}_G$  are the modal masses, of translational and rotational kind, respectively;  $K_x, K_y, K_\vartheta$  are the modal stiffnesses;  $\xi_x, \xi_y, \xi_\vartheta$  the modal damping ratios;  $c_d, c_l, c_m$  the drag, lift and moment aerodynamic coefficients, respectively, with  $c'_l, c'_m$  their derivatives with respect the angle of attack;  $\rho_a$  is the air density;  $b$  is a characteristic length of



the cross-section and  $R$  its characteristic twist radius (e.g., [8]); finally,  $L$  is the length of the cylinder. The constant forces due to the mean wind velocity have been neglected; furthermore, the effect of atmospheric turbulence has not been explicitly considered, even if it could be approximately recovered through suitably modified aerodynamic coefficients (e.g., [4]). The explicit influence of turbulence is potentially important for tall, large building and towers; for slender towers in boundary-layer winds an increasing turbulence intensity can lead to a decrease in the standard deviation of the response in the dominant mode [10].

Equations (1) can also be interpreted as the equations of a sectional model, to be tested in wind tunnel, where  $M, \mathcal{J}_G$  are the masses of the cylinder (of length  $L$ ) and  $K_x, K_y, K_\vartheta$  are the stiffnesses of the springs supporting the body (see Fig 1). Due to the double symmetry, all the structural matrices are diagonal, while the aerodynamic matrices are non-diagonal, providing coupling between the cross-wind motion  $v(t)$  and the twist  $\vartheta(t)$ . The along-wind motion  $u(t)$ , instead, being uncoupled and damped, decays in time, so that it can be ignored in the galloping analysis. Similar considerations on the decoupling of the problem could be made, albeit in an approximate way, even in the absence of symmetry, in the case in which the along-wind oscillations occur at a very different frequency compared to the other two directions.

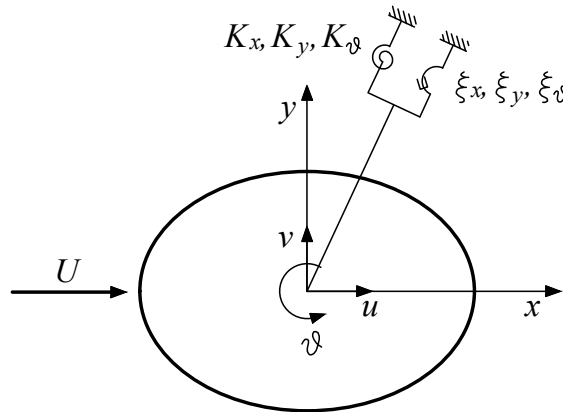


Figure 1. Sectional model.

The following assumptions, holding throughout the paper, are made, concerning the signs of the aerodynamic coefficients:

$$c'_l < 0, \quad |c'_l| > c_d > 0, \quad c'_m > 0 \tag{3}$$

The first two conditions, make it possible the cylinder instabilizes in the flexural mode (when twist is suppressed) at a sufficiently high wind velocity; the last condition makes positive the torsional aerodynamic stiffness, in order to exclude torsional divergence (when translation is prevented), while allowing torsional galloping to occur. As an example, the squared cross-section satisfies these properties (e.g., [14]).

To transform the equation of motion (1) in a nondimensional form, the following quantities are introduced:

$$\begin{aligned} \alpha_{yy} &:= 2\xi_y + \mu\eta_y (c_d + c'_l), & \alpha_{y\vartheta} &:= -\mu\eta_y \frac{R}{b} (c_d + c'_l), \\ \alpha_{\vartheta y} &:= \mu\eta_\vartheta c'_m, & \alpha_{\vartheta\vartheta}(\Omega) &:= 2\xi_\vartheta \Omega - \mu\eta_\vartheta \frac{R}{b} c'_m, \\ \beta_{y\vartheta} &:= \mu^2 \eta_y c'_l, & \beta_{\vartheta\vartheta} &:= \mu^2 \eta_\vartheta c'_m, \\ \eta_y &:= \frac{\rho_a b^2 L}{2M}, & \eta_\vartheta &:= \frac{\rho_a b^4 L}{2\mathcal{J}_G} \\ \tilde{v} &:= \frac{v}{b}, & \tilde{t} &:= \omega_y t, \\ \mu &:= \frac{U}{\omega_y b}, & \Omega &:= \frac{\omega_\vartheta}{\omega_y}, \end{aligned} \tag{4}$$

where  $\omega_y := \sqrt{\frac{K_y}{M}}$ ,  $\omega_\vartheta := \sqrt{\frac{K_\vartheta}{\mathcal{J}_G}}$  are the natural flexural and torsional frequency, respectively. Here,  $\alpha_{ij}$  are nondimensional coefficients of the velocity-dependent forces (i.e., of the motion-induced forces which are in-phase with the local velocity of the moving object);  $\beta_{ij}$  are nondimensional coefficients of the positional forces (i.e., of the out-of-phase components of the motion-induced forces);  $\Omega$  is the torsional-to-flexural frequency ratio;  $\mu$  is the nondimensional wind velocity, which differs from the definition of the reduced wind speed by a scalar factor  $2\pi$  (see Sect 1). All  $\alpha_{ij}, \beta_{ij}$  depend on  $\mu$  (dependence understood); in addition,  $\alpha_{\vartheta\vartheta}$  also depends on  $\Omega$  (dependence made explicit).

With the positions (4), the equations governing the flexural-torsional motions are recast in the form:

$$\begin{pmatrix} 1 & 0 \\ 0 & 1 \end{pmatrix} \begin{pmatrix} \ddot{v} \\ \ddot{\vartheta} \end{pmatrix} + \begin{pmatrix} \alpha_{yy} & \alpha_{y\vartheta} \\ \alpha_{\vartheta y} & \alpha_{\vartheta\vartheta}(\Omega) \end{pmatrix} \begin{pmatrix} \dot{v} \\ \dot{\vartheta} \end{pmatrix} + \begin{pmatrix} 1 & \beta_{y\vartheta} \\ 0 & \Omega^2 + \beta_{\vartheta\vartheta} \end{pmatrix} \begin{pmatrix} v \\ \vartheta \end{pmatrix} = \begin{pmatrix} 0 \\ 0 \end{pmatrix} \tag{5}$$

where the tilde has been omitted, and the dot denotes differentiation with respect the nondimensional time.

### 3. Exact solution

The Eqs (5) admit the particular solution:

$$\begin{pmatrix} v \\ \vartheta \end{pmatrix} = \begin{pmatrix} \hat{v} \\ \hat{\vartheta} \end{pmatrix} \exp(\lambda t) \tag{6}$$



in which  $(\hat{v}, \hat{\vartheta})^T$  is an eigenvector and  $\lambda$  is an eigenvalue of the following algebraic problem:

$$\left( \lambda^2 \begin{pmatrix} 1 & 0 \\ 0 & 1 \end{pmatrix} + \lambda \begin{pmatrix} \alpha_{yy} & \alpha_{y\vartheta} \\ \alpha_{\vartheta y} & \alpha_{\vartheta\vartheta}(\Omega) \end{pmatrix} + \begin{pmatrix} 1 & \beta_{y\vartheta} \\ 0 & \Omega^2 + \beta_{\vartheta\vartheta} \end{pmatrix} \right) \begin{pmatrix} \hat{v} \\ \hat{\vartheta} \end{pmatrix} = \begin{pmatrix} 0 \\ 0 \end{pmatrix} \tag{7}$$

Since the matrix of the coefficients is non-symmetric, both the eigenvectors and the eigenvalues are, in general, complex. The characteristic equation of the problem is:

$$p(\lambda) := \lambda^4 + \lambda^3 (\alpha_{yy} + \alpha_{\vartheta\vartheta}) + \lambda^2 (1 + \Omega^2 - \alpha_{y\vartheta}\alpha_{\vartheta y} + \alpha_{yy}\alpha_{\vartheta\vartheta} + \beta_{\vartheta\vartheta}) + \lambda (\Omega^2\alpha_{yy} + \alpha_{\vartheta\vartheta} - \alpha_{\vartheta y}\beta_{y\vartheta} + \alpha_{yy}\beta_{\vartheta\vartheta}) + \Omega^2 + \beta_{\vartheta\vartheta} = 0 \tag{8}$$

### 3.1 Linear stability analysis

A linear stability analysis is carried out in the parameter space  $(\mu, \Omega)$ . Here,  $\mu$  is the distinguished parameter, and  $\Omega$  is the splitting parameter (since it splits the resonance and possible double Hopf bifurcations).

A (simple) Hopf bifurcation occurs when, by increasing the bifurcation parameter  $\mu$ , a pair of complex conjugate eigenvalues crosses the imaginary axis from the left. Therefore, at the incipient bifurcation, Eq (8) admits the root  $\lambda = i\omega$ , with  $\omega$  unknown. By substituting it in the equation and separating real and imaginary parts, two real equations are obtained:

$$\Omega^2 + \beta_{\vartheta\vartheta} - \omega^2 - \Omega^2\omega^2 + \alpha_{y\vartheta}\alpha_{\vartheta y}\omega^2 - \alpha_{yy}\alpha_{\vartheta\vartheta}(\Omega)\omega^2 - \beta_{\vartheta\vartheta}\omega^2 + \omega^4 = 0 \tag{9}$$

$$\omega [\Omega^2\alpha_{yy} + \alpha_{\vartheta\vartheta}(\Omega) - \alpha_{\vartheta y}\beta_{y\vartheta} + \alpha_{yy}\beta_{\vartheta\vartheta} - \omega^2(\alpha_{yy} + \alpha_{\vartheta\vartheta}(\Omega))] = 0 \tag{10}$$

Equation (10) can be solved to supply  $\omega = \omega(\mu; \Omega)$ , leading to:

$$\omega_1 = 0 \tag{11}$$

$$\omega_{2,3} = \pm \sqrt{\frac{\Omega^2\alpha_{yy} + \alpha_{\vartheta\vartheta} - \alpha_{\vartheta y}\beta_{y\vartheta} + \alpha_{yy}\beta_{\vartheta\vartheta}}{\alpha_{yy} + \alpha_{\vartheta\vartheta}(\Omega)}} \tag{12}$$

When the first root,  $\omega_1 = 0$ , is substituted in Eq (9),  $\Omega^2 + \beta_{\vartheta\vartheta}(\mu) = 0$  is found, i.e. the condition for which the stiffness matrix is singular. In this occurrence, a torsional divergence manifests at the critical wind velocity  $\mu_d := \Omega/\sqrt{-\eta\vartheta c'_m}$ , requiring  $c'_m < 0$  (destabilizing aerodynamic torsional stiffness). In this paper, however, this case will be excluded by the assumption that the torsional effect is stabilizing, Eq (3) (i.e.  $c'_m > 0$ ).

When  $\omega_{2,3}$  is substituted in Eq (9), an algebraic equation of fifth degree in  $\Omega$  is found, namely:

$$p_1(\Omega)\Omega^4 + p_2(\Omega)\Omega^2 + p_3(\Omega) = 0 \tag{13}$$

whose coefficients  $p_i(\Omega)$  are polynomials of  $\Omega$ , whose expressions are reported in the Appendix A (Eqs (77)). Equation (13) calls for a numerical solution. For any value of  $\mu$ , five roots  $\Omega$  are found, among which only the real and positive ones are kept. The graph of the roots in the  $(\Omega, \mu)$  parameter plane (linear stability diagram) is a geometrical locus representative of a family of systems (parameterized by  $\Omega$ ) at the incipient instability condition. The points of the plane below the lowest critical curve constitute the stability domain.

At the stability boundary, the Hopf frequency  $\omega$  (i.e. the frequency of limit-cycle about to be born there) is evaluated by Eq (12); the eigenvector, from Eq (7), is:

$$(\hat{v}, \hat{\vartheta})^T = \left( 1, \frac{(-\beta_{y\vartheta} + \omega^2\beta_{y\vartheta} - \omega^2\alpha_{yy}\alpha_{y\vartheta}) + i\omega(\alpha_{y\vartheta} - \alpha_{yy}\beta_{y\vartheta} - \omega^2\alpha_{y\vartheta})}{\beta_{y\vartheta}^2 + \omega^2\alpha_{y\vartheta}^2} \right)^T \tag{14}$$

in which  $\hat{v} = 1$  has been taken for normalization. Since the mode is complex, the trajectory experienced by the system in the  $(v, \vartheta)$  configuration space is elliptical, of parametric equations:

$$\begin{pmatrix} v \\ \vartheta \end{pmatrix} = \begin{pmatrix} 1 \\ \text{Re}(\hat{\vartheta}) \end{pmatrix} \cos(\omega t) - \begin{pmatrix} 0 \\ \text{Im}(\hat{\vartheta}) \end{pmatrix} \sin(\omega t) \tag{15}$$

(to within an unessential scaling factor).

### 3.2 Double-Hopf bifurcation points

The possible occurrence of Double-Hopf (DH) bifurcation points is explored. At these DH-points, two pairs of complex eigenvalues,  $\lambda = \pm i\omega_1, \pm i\omega_2$ , simultaneously cross the imaginary axis, when the distinguished bifurcation parameter is increased. The phenomenon is potentially dangerous, since it leads, in the nonlinear field, to a complex dynamics in which periodic and quasi-periodic motions compete among them (see, e.g., [31, 32]). At a DH point, the characteristic equation reads  $p(\lambda) = (\lambda^2 + \omega_1^2)(\lambda^2 + \omega_2^2)$ ; by equating it to the general expression (8), four real equations are drawn, i.e.:

$$\alpha_{yy} + \alpha_{\vartheta\vartheta}(\Omega) = 0 \tag{16}$$

$$1 + \Omega^2 - \alpha_{y\vartheta}\alpha_{\vartheta y} + \alpha_{yy}\alpha_{\vartheta\vartheta}(\Omega) + \beta_{\vartheta\vartheta} = \omega_1^2 + \omega_2^2 \tag{17}$$

$$\Omega^2\alpha_{yy} + \alpha_{\vartheta\vartheta}(\Omega) - \alpha_{\vartheta y}\beta_{y\vartheta} + \alpha_{yy}\beta_{\vartheta\vartheta} = 0 \tag{18}$$

$$\Omega^2 + \beta_{\vartheta\vartheta} = \omega_1^2\omega_2^2 \tag{19}$$



Equation (16), after using the definitions (4), can be solved for linking the  $\Omega$  and  $\mu$  parameters, thus obtaining:

$$\mu(\Omega) = -\frac{2(\xi_y + \xi_\vartheta \Omega)}{\eta_y(c_d + c'_l) - \eta_\vartheta \frac{R}{b} c'_m} \tag{20}$$

By substituting it into Eq (18), a cubic equation is found for the unknown  $\Omega$ :

$$J_0 \Omega^3 + J_1 \Omega^2 + J_2 \Omega + J_3 = 0 \tag{21}$$

whose coefficients are reported in Appendix A (Eqs (78)). Any real positive solution  $\Omega$  of Eq (21), together with the associated  $\mu$  given by Eq (20), selects a DH point in the parameter plane.

By using the remaining Eqs (17), (19), the Hopf frequencies  $\omega_1, \omega_2$  can be evaluated. Usually, they are uncommensurable, so that the bifurcation is non-resonant. If, however, a third parameter were considered (for example by exploring a family of aerodynamic coefficients), a resonant DH bifurcation could occur, as for example studied in [33, 34, 35].

### 4. Perturbation analysis

Although the exact analysis developed above gives exhaustive answers to the stability problem, it cannot highlight the mechanism of coupling, which is somewhat related to the resonance between flexural and torsional degrees of freedom. Moreover, since it would be desirable to obtain closed-form solutions for the eigenvalue problem (7), a perturbation analysis is carried out. Two cases are examined: non resonant problem ( $\Omega \neq 1$ ) and resonant problem ( $\Omega \simeq 1$ ), each of which calling for a different perturbation expansion.

#### 4.1 Non resonant problem ( $\Omega \neq 1$ )

In starting a perturbation analysis, it needs to estimate the order of magnitude of the different terms, parameters and unknowns. Such an ordering, of course, has to be checked *a posteriori*, in the sense that the perturbation solution is valid in the range in which the unknowns assume the expected values. In the problem at hands, all  $\alpha_{ij}, \beta_{ij}$  depend on  $\mu$ , whose critical value is unknown. An estimation of the expected  $\mu$  is performed here, suggested by the following conjectures.

If any coupling between the two degree of freedoms were ignored, either: (i) flexural galloping would manifest at the wind velocity  $\mu_y$ , such that  $\alpha_{yy} = 0$ ; or (ii) torsional galloping would occur at wind velocity  $\mu_\vartheta$ , such that  $\alpha_{\vartheta\vartheta} = 0$ . Both the conditions denote vanishing of the total (structural plus aerodynamic) damping, according to the well-known Den Hartog criterion. By using Eqs (4), these velocities are:

$$\mu_y := -\frac{2\xi_y}{\eta_y(c_d + c'_l)} \tag{22}$$

$$\mu_\vartheta(\Omega) := \frac{2\xi_\vartheta \Omega}{\eta_\vartheta \frac{R}{b} c'_m} \tag{23}$$

They are both positive, according to the properties (3). Equations (22)-(23) describe two straight lines in the  $(\mu, \Omega)$  parameter plane.

Far from resonance, and when  $\Omega > 1$ , it is expected that coupling is weak, so that the critical velocity is close to that of Den Hartog, i.e.  $\mu \simeq \mu_y$ . Since the quasi-steady theory is believed to hold at the reduced velocities  $2\pi \frac{U}{\omega_y b} \equiv 2\pi\mu > 20$  (for square or compact sections, e.g. [4]), it is guessed that  $\mu^2 = O(10)$ . Since the key-term  $\beta_{y\vartheta}$  of the aerodynamic stiffness, responsible for the coupling, is proportional to  $\mu^2$ , it is likely to enter among the leading terms of the eigenvalue problem, at the same order of the elastic stiffnesses. The other stiffness term,  $\beta_{\vartheta\vartheta}$ , is usually smaller, but it can be checked that, considering it of the same order of  $\beta_{y\vartheta}$ , while simplifying the analysis, does not entail significant errors. On the contrary, since the damping terms  $\alpha_{ij}$  linearly depend on  $\mu$ , and some of them nearly vanishes at the bifurcation, they should be considered as small perturbations. In conclusion, the following ordering is conjectured:  $\alpha_{ij} = O(\epsilon), \beta_{ij} = O(1)$ , where  $\epsilon$  is a perturbation parameter. By rescaling  $\alpha_{ij} \rightarrow \epsilon\alpha_{ij}$ , the eigenvalue problem (7) becomes:

$$\left( \begin{pmatrix} 1 + \lambda^2 & \beta_{y\vartheta} \\ 0 & \Omega^2 + \beta_{\vartheta\vartheta} + \lambda^2 \end{pmatrix} + \epsilon\lambda \begin{pmatrix} \alpha_{yy} & \alpha_{y\vartheta} \\ \alpha_{\vartheta y} & \alpha_{\vartheta\vartheta}(\Omega) \end{pmatrix} \right) \begin{pmatrix} \hat{v} \\ \hat{\vartheta} \end{pmatrix} = \begin{pmatrix} 0 \\ 0 \end{pmatrix} \tag{24}$$

The eigenvalues  $\lambda$  and eigenvectors  $\mathbf{u} := (\hat{v}, \hat{\vartheta})^T$ , all depending on  $\epsilon$ , are expanded in series as follows:

$$\lambda = \lambda_0 + \epsilon\lambda_1 + \dots \tag{25}$$

$$\begin{pmatrix} \hat{v} \\ \hat{\vartheta} \end{pmatrix} = \begin{pmatrix} \hat{v}_0 \\ \hat{\vartheta}_0 \end{pmatrix} + \epsilon \begin{pmatrix} \hat{v}_1 \\ \hat{\vartheta}_1 \end{pmatrix} + \dots \tag{26}$$

where the coefficients are all unknowns. By substituting them in Eq (24), and separately equating to zero the coefficients of the same power of  $\epsilon$ , the following perturbation equations, up to the  $\epsilon$ -order, are obtained:

Order  $\epsilon^0$ :

$$\begin{pmatrix} 1 + \lambda_0^2 & \beta_{y\vartheta} \\ 0 & \Omega^2 + \beta_{\vartheta\vartheta} + \lambda_0^2 \end{pmatrix} \begin{pmatrix} \hat{v}_0 \\ \hat{\vartheta}_0 \end{pmatrix} = \begin{pmatrix} 0 \\ 0 \end{pmatrix} \tag{27}$$

Order  $\epsilon^1$ :

$$\begin{pmatrix} 1 + \lambda_0^2 & \beta_{y\vartheta} \\ 0 & \Omega^2 + \beta_{\vartheta\vartheta} + \lambda_0^2 \end{pmatrix} \begin{pmatrix} \hat{v}_1 \\ \hat{\vartheta}_1 \end{pmatrix} = -\lambda_0 \begin{pmatrix} \alpha_{yy} + 2\lambda_1 & \alpha_{y\vartheta} \\ \alpha_{\vartheta y} & \alpha_{\vartheta\vartheta}(\Omega) + 2\lambda_1 \end{pmatrix} \begin{pmatrix} \hat{v}_0 \\ \hat{\vartheta}_0 \end{pmatrix} \tag{28}$$

The lower-order generating problem (27) admits two eigensolutions (and their complex conjugates), namely:

(F) Flexural mode:

$$\lambda_0^F = i, \quad \mathbf{u}_0^F = (1, 0)^T \tag{29}$$



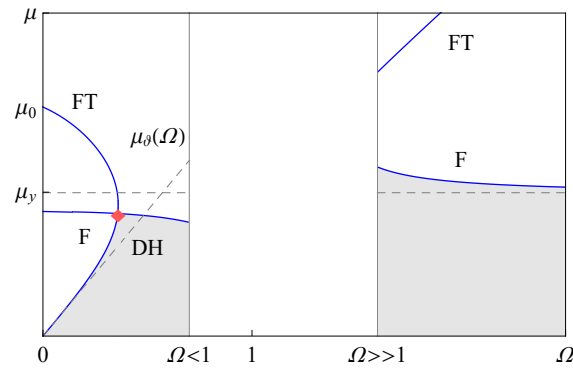


Figure 2. A sketch of the loci of incipient instability for small and large values of  $\Omega$ ; shaded area stable.

(FT) Flexural-Torsional mode:

$$\lambda_0^{FT} = i\sqrt{\Omega^2 + \beta_{\vartheta\vartheta}}, \quad \mathbf{u}_0^{FT} = \left( 1, \frac{\Omega^2 - 1 + \beta_{\vartheta\vartheta}}{\beta_{yy\vartheta}} \right)^T \tag{30}$$

From this first step it appears clear that, due to the nature of aerodynamic stiffness, the critical mode is a perturbation of either the (F) or the (FT) modes; hence, torsion never prevails over flexure.

When the (F)-solution (29) is substituted in Eq (28), this latter reads:

$$\begin{pmatrix} 0 & \beta_{y\vartheta} \\ 0 & \Omega^2 - 1 + \beta_{\vartheta\vartheta} \end{pmatrix} \begin{pmatrix} \hat{v}_1 \\ \hat{\vartheta}_1 \end{pmatrix} = -i \begin{pmatrix} \alpha_{yy} + 2\lambda_1 \\ \alpha_{\vartheta y} \end{pmatrix} \tag{31}$$

Since the matrix of the coefficients is singular, according to the Rouché-Capelli Theorem,  $\lambda_1$  must satisfy a compatibility (or solvability) condition, supplying:

$$\lambda_1^F = \frac{1}{2} \left( -\alpha_{yy} + \beta_{y\vartheta} \frac{\alpha_{\vartheta y}}{\Omega^2 - 1 + \beta_{\vartheta\vartheta}} \right) \tag{32}$$

which is a purely real correction of the imaginary eigenvalue  $\lambda_0^F$ . By solving the equations (31):

$$\mathbf{u}_1^F = \left( 0, -i \frac{\alpha_{\vartheta y}}{\Omega^2 - 1 + \beta_{\vartheta\vartheta}} \right)^T \tag{33}$$

is found, where  $\hat{v}_1 = 0$  has been taken as normalization condition; it is a purely imaginary correction of the real eigenvector  $\mathbf{u}_0^F$ .

When the (FT)-solution (30) is substituted in Eq (28), this latter reads:

$$\begin{pmatrix} 1 - (\Omega^2 + \beta_{\vartheta\vartheta}) & \beta_{y\vartheta} \\ 0 & 0 \end{pmatrix} \begin{pmatrix} \hat{v}_1 \\ \hat{\vartheta}_1 \end{pmatrix} = -i\sqrt{\Omega^2 + \beta_{\vartheta\vartheta}} \begin{pmatrix} \alpha_{yy} + 2\lambda_1 & \alpha_{y\vartheta} \\ \alpha_{\vartheta y} & \alpha_{\vartheta\vartheta}(\Omega) + 2\lambda_1 \end{pmatrix} \begin{pmatrix} 1 \\ \frac{\Omega^2 - 1 + \beta_{\vartheta\vartheta}}{\beta_{yy\vartheta}} \end{pmatrix} \tag{34}$$

Solvability establishes that:

$$\lambda_1^{FT} = -\frac{1}{2} \left( \alpha_{\vartheta\vartheta}(\Omega) + \frac{\alpha_{\vartheta y}\beta_{y\vartheta}}{\Omega^2 - 1 + \beta_{\vartheta\vartheta}} \right) \tag{35}$$

which is a purely real correction of the imaginary eigenvalue  $\lambda_0^{FT}$ . The normalized solution of Eq (34) is:

$$\mathbf{u}_1^{FT} = \left( 0, i\sqrt{\Omega^2 + \beta_{\vartheta\vartheta}} \left( \frac{2\lambda_1^{FT} + \alpha_{yy}}{\beta_{yy\vartheta}} + \frac{\alpha_{y\vartheta}(\Omega^2 - 1 + \beta_{\vartheta\vartheta})}{\beta_{yy\vartheta}^2} \right) \right)^T \tag{36}$$

which is a purely imaginary correction of the real eigenvector  $\mathbf{u}_0^{FT}$ .

By coming back to the series expansion (25), since  $\text{Re}(\lambda_0 + \epsilon\lambda_1) = \epsilon\lambda_1$  for both the (F) and (FT) modes, stability is governed by the  $\epsilon$ -order part of the eigenvalues. Consequently, by letting  $\lambda_1 = 0$ , since it depends on  $(\mu, \Omega)$ , the geometrical locus of incipient bifurcation is found on the parameter plane. Concerning the (F) mode,  $\lambda_1^F = 0$  (Eq 32) entails:

$$\Omega^2(\mu) = 1 - \beta_{\vartheta\vartheta} + \frac{\alpha_{\vartheta y}\beta_{y\vartheta}}{\alpha_{yy}} \tag{37}$$

This is a closed-form expression for the curve  $\Omega = \Omega(\mu)$ ; its asymptotic character for  $\Omega \rightarrow +\infty$  or  $\Omega \rightarrow 0$  are analyzed (see Fig 2 for a sketch). When  $\Omega \rightarrow +\infty$ , since  $\alpha_{\vartheta y}\beta_{y\vartheta} < 0$ , then  $\alpha_{yy} \rightarrow 0^-$ , i.e.  $\mu \rightarrow \mu_y^+$ ; therefore, the Den Hartog value  $\mu_y$ , Eq (22), is recovered from above. It is confirmed that, far from resonance, the system behaves as uncoupled. Close to  $\Omega = 0$ , instead,  $\alpha_{yy} \simeq \frac{\alpha_{\vartheta y}\beta_{y\vartheta}}{\beta_{\vartheta\vartheta} - 1}$ ; then, so far  $\beta_{\vartheta\vartheta} < 1$ , it is  $\alpha_{yy} > 0$ , which means that galloping occurs at a critical value  $\mu < \mu_y$ , i.e. coupling has a detrimental effect on flexural galloping.

Concerning the (FT) mode,  $\lambda_1^{FT} = 0$  (Eq 35) leads to:

$$(\Omega^2 - 1 + \beta_{\vartheta\vartheta}) \alpha_{\vartheta\vartheta}(\Omega) + \alpha_{\vartheta y}\beta_{y\vartheta} = 0 \tag{38}$$

which is a cubic equation for  $\Omega = \Omega(\mu)$ , generally calling for a numerical solution. However, asymptotic information can be got for  $\Omega \ll 1$ , or  $\Omega \gg 1$ , for which the following solutions hold (see Appendix B for details, and Fig 2 for a sketch):



$$\Omega \simeq \begin{cases} \frac{1}{2\xi_\vartheta} \left( \mu\eta_\vartheta \frac{R}{b} c'_m + \mu^3 \frac{\eta_y^2 \frac{R}{b} c'_l (c_d + c'_l)}{1 - \mu^2 \eta_\vartheta c'_m} \right) & \text{when } \Omega \ll 1 \\ \left[ \frac{R}{b} \frac{\eta_\vartheta}{2\xi_\vartheta} c'_m + \left( \frac{b}{R} \right)^2 \frac{2\xi_\vartheta}{\eta_\vartheta} \frac{\eta_y c'_l}{c'_m} \right] \mu & \text{when } \Omega \gg 1 \end{cases} \quad (39)$$

These expressions entail that: (i) the plot of  $\Omega(\mu)$  is a curve passing through the origin, since, for the mechanical model adopted,  $\omega_\vartheta = 0$  entails  $\xi_\vartheta = 0$ ; (ii)  $\Omega(\mu)$  is tangent at the origin to the straight line  $\alpha_{\vartheta\vartheta} = 0$ , i.e.  $\mu \simeq \mu_\vartheta(\Omega)$ ; (iii) in addition to the origin,  $\Omega(\mu)$  crosses the  $\mu$ -axis at a non-zero  $\mu_0$  value, denoting a successive bifurcation; (iv)  $\Omega(\mu)$  is a straight line far from the origin, whose angular coefficient, by virtue of Eq (3), is less than that  $\alpha_{\vartheta\vartheta} = 0$ . The plot of Fig 2 highlights the stable domain (shaded area) and the occurrence of a DH-point (red symbol) in the range  $\Omega < 1$ .

Finally, is it worth noticing that, far from  $\Omega = 1$  and due to the perturbation method, the five-degree algebraic equation (13) is broken into two equations, one of second-degree (Eq (37)), the other of third-degree (Eq (38)).

**4.2 Resonant problem ( $\Omega \simeq 1$ )**

The non-resonant solution does not hold when  $\Omega^2 + \beta_{\vartheta\vartheta} \simeq 1$ , i.e. when the modified torsional frequency, accounting for the (usually small) aerodynamic stiffness, is close to the flexural frequency. In this case, a resonance occurs between the two degrees of freedom. Indeed, since the denominator in the Eqs (32), (35) tends to zero, in order that  $\lambda_1$  does not diverge to infinity, also  $\mu$  must tend to zero. Thus, a quite unrealistic occurrence it depicted, i.e. that the critical load tends to zero at the resonance. It will be proved, in the following, that this wrong information is a consequence of a wrong ordering of the coefficients in the equation of motion (1). Indeed, when  $\mu \rightarrow 0$ , the coupling coefficient  $\beta_{y\vartheta}$  tends to zero, too. Therefore, for  $\mu$  small, it must be ordered at the higher-order  $\epsilon$ , and not more included among the leading terms, as done in Eq (24). By performing the same rescaling for the companion coefficients, the ordering  $\beta_{ij} \rightarrow \epsilon\beta_{ij}$  is performed, still keeping  $\alpha_{ij} \rightarrow \epsilon\alpha_{ij}$ . Moreover, to express the closeness of  $\Omega$  to 1, a detuning parameter  $\sigma$  is introduced, such that:

$$\Omega = 1 + \epsilon\sigma \quad (40)$$

Hence, the eigenvalue problem (7) is recast in the form:

$$\left( \begin{pmatrix} 1 + \lambda^2 & 0 \\ 0 & 1 + \lambda^2 \end{pmatrix} + \epsilon \begin{pmatrix} \lambda\alpha_{yy} & \beta_{y\vartheta} + \lambda\alpha_{y\vartheta} \\ \lambda\alpha_{\vartheta y} & 2\sigma + \beta_{\vartheta\vartheta} + \lambda\alpha_{\vartheta\vartheta}(1) \end{pmatrix} \right) \begin{pmatrix} \hat{v} \\ \hat{\vartheta} \end{pmatrix} = \begin{pmatrix} 0 \\ 0 \end{pmatrix} \quad (41)$$

where  $\epsilon\alpha_{\vartheta\vartheta}(\theta) = \epsilon\alpha_{\vartheta\vartheta}(1) + O(\epsilon^2)$  has been used. The eigenvalue  $\lambda(\epsilon)$  appears as a perturbation of a semisimple double eigenvalue  $\lambda(0) = \pm i$  (i.e. a double root admitting two independent eigenvectors). The relevant perturbation algorithm is applied (see, e.g., [36, 37]).

By using the same expansions (25)-(26) of the non-resonant case, the following perturbation equations are derived:  
Order  $\epsilon^0$

$$\begin{pmatrix} 1 + \lambda_0^2 & 0 \\ 0 & 1 + \lambda_0^2 \end{pmatrix} \begin{pmatrix} \hat{v}_0 \\ \hat{\vartheta}_0 \end{pmatrix} = \begin{pmatrix} 0 \\ 0 \end{pmatrix} \quad (42)$$

Order  $\epsilon^1$

$$\begin{pmatrix} 1 + \lambda_0^2 & 0 \\ 0 & 1 + \lambda_0^2 \end{pmatrix} \begin{pmatrix} \hat{v}_1 \\ \hat{\vartheta}_1 \end{pmatrix} = - \begin{pmatrix} \lambda_0\alpha_{yy} + 2\lambda_0\lambda_1 & \beta_{y\vartheta} + \lambda_0\alpha_{y\vartheta} \\ \lambda_0\alpha_{\vartheta y} & 2\sigma + \beta_{\vartheta\vartheta} + \lambda_0\alpha_{\vartheta\vartheta}(1) + 2\lambda_0\lambda_1 \end{pmatrix} \begin{pmatrix} \hat{v}_0 \\ \hat{\vartheta}_0 \end{pmatrix} \quad (43)$$

The generating perturbation equation (42) admits the double root  $\lambda_0 = i$  (and its complex conjugate). Infinite eigenvectors, spanning a plane, are associated with  $\lambda_0$ :

$$\begin{pmatrix} \hat{v}_0 \\ \hat{\vartheta}_0 \end{pmatrix} = a_1 \begin{pmatrix} 1 \\ 0 \end{pmatrix} + a_2 \begin{pmatrix} 0 \\ 1 \end{pmatrix} \quad (44)$$

where  $a_1, a_2$  are arbitrary constants. To resolve indeterminacy, it needs to go to the  $\epsilon$ -order. With the previous results, the Eq (43) reads:

$$\begin{pmatrix} 0 & 0 \\ 0 & 0 \end{pmatrix} \begin{pmatrix} \hat{v}_1 \\ \hat{\vartheta}_1 \end{pmatrix} = -i \begin{pmatrix} \alpha_{yy} + 2\lambda_1 & \alpha_{y\vartheta} - i\beta_{y\vartheta} \\ \alpha_{\vartheta y} & \alpha_{\vartheta\vartheta} - i\beta_{\vartheta\vartheta} - 2i\sigma + 2\lambda_1 \end{pmatrix} \begin{pmatrix} a_1 \\ a_2 \end{pmatrix} \quad (45)$$

Solvability requires the right hand member vanishes, from which a new eigenvalue problem in  $\lambda_1$  is drawn, whose characteristic equation is:

$$4\lambda_1^2 + \lambda_1 (2\text{tr}\mathbf{A} - 2i\beta_{\vartheta\vartheta} - 4i\sigma) + \det\mathbf{A} + i\alpha_{\vartheta y}\beta_{y\vartheta} - i\alpha_{y\vartheta}\beta_{\vartheta\vartheta} - 2i\alpha_{yy}\sigma = 0 \quad (46)$$

where  $\text{tr}\mathbf{A} := \alpha_{yy} + \alpha_{\vartheta\vartheta}(1)$  and  $\det\mathbf{A} := \alpha_{yy}\alpha_{\vartheta\vartheta}(1) - \alpha_{y\vartheta}\alpha_{\vartheta y}$  are trace and determinant, respectively, of the aerodynamic and structural damping matrix  $\mathbf{A} := [\alpha_{ij}]$ , evaluated at  $\Omega = 1$ .

On the stability boundary,  $\text{Re}(\lambda_1) = 0$ , i.e.  $\lambda_1 = i\omega_1$  (with  $\omega_1$  the unknown Hopf frequency). Substituting it in Eq (46) and separating real and imaginary parts, two real equations follow:

$$-4\omega_1^2 + 2\omega_1 (\beta_{\vartheta\vartheta} + 2\sigma) + \det\mathbf{A} = 0 \quad (47)$$

$$2\omega_1 \text{tr}\mathbf{A} + \alpha_{\vartheta y}\beta_{y\vartheta} - \alpha_{yy} (\beta_{\vartheta\vartheta} + 2\sigma) = 0 \quad (48)$$

From Eq (48),  $\omega_1$  is expressed in terms of  $\sigma$  and  $\mu$ :

$$\omega_1 = - \frac{\alpha_{\vartheta y}\beta_{y\vartheta} - \alpha_{yy} (\beta_{\vartheta\vartheta} + 2\sigma)}{2\text{tr}\mathbf{A}} \quad (49)$$

When it is substituted into Eq (47), a quadratic equation for the detuning is derived, namely:

$$[\alpha_{\vartheta y}\beta_{y\vartheta} - \alpha_{yy} (\beta_{\vartheta\vartheta} + 2\sigma)] [\alpha_{\vartheta y}\beta_{y\vartheta} + (\beta_{\vartheta\vartheta} + 2\sigma) \alpha_{\vartheta\vartheta}(1)] - \det\mathbf{A} \text{tr}^2\mathbf{A} = 0 \quad (50)$$

or:

$$I_0\sigma^2 + I_1\sigma + I_2 = 0 \quad (51)$$



where the ( $\mu$ -dependent) coefficients  $I_j$  are:

$$I_0 := 4\alpha_{yy}\alpha_{\vartheta\vartheta} (1) \tag{52}$$

$$I_1 := 2\alpha_{\vartheta y}\beta_{y\vartheta} (\alpha_{yy} - \alpha_{\vartheta\vartheta} (1)) + 4\alpha_{yy}\alpha_{\vartheta\vartheta} (1)\beta_{\vartheta\vartheta} \tag{53}$$

$$I_2 := \det \mathbf{A} \operatorname{tr}^2 \mathbf{A} - \alpha_{\vartheta y}^2 \beta_{y\vartheta}^2 + \beta_{\vartheta\vartheta} \alpha_{\vartheta y} \beta_{y\vartheta} (\alpha_{yy} - \alpha_{\vartheta\vartheta} (1)) + \beta_{\vartheta\vartheta}^2 \alpha_{yy} \alpha_{\vartheta\vartheta} (1) \tag{54}$$

From Eqs (51) two solutions for  $\sigma(\mu)$  are obtained:

$$\sigma^\pm(\mu) = \frac{-I_1 \pm \sqrt{I_1^2 - 4I_0 I_2}}{2I_0} \tag{55}$$

If they are real, two values for the Hopf frequency  $\omega_1^\pm(\mu)$  are derived from Eq (49), and two values for the frequency ratio are drawn from Eq (40), with the parameter  $\epsilon$  reabsorbed:

$$\Omega^\pm(\mu) = 1 + \sigma^\pm(\mu) \tag{56}$$

It is observed that:

1. At  $\mu = \mu_y$ , or  $\mu = \mu_{\vartheta} (1)$ , it is  $\alpha_{yy} = 0$  or  $\alpha_{\vartheta\vartheta} (1) = 0$ , respectively, so that  $I_0 = 0$ . One of the two roots  $\sigma$  of Eq (51), consequently, tends to infinity, i.e. the graph of  $\Omega(\mu)$  has two horizontal asymptotes.
2. When  $\beta_{y\vartheta} = O(1)$ ,  $\beta_{\vartheta\vartheta} = O(1)$  together with  $\sigma = O(1)$ , i.e. the ordering of the resonance analysis is violated, the resonant solution recovers the non-resonant solution. Indeed, the factorized expression (50) of the second-degree equation (51) brakes in two linear equations, supplying:

$$\sigma^- = \frac{1}{2} \frac{\alpha_{\vartheta y} \beta_{y\vartheta}}{\alpha_{yy}} - \beta_{\vartheta\vartheta}, \quad \sigma^+ = -\frac{1}{2} \frac{\alpha_{\vartheta y} \beta_{y\vartheta}}{\alpha_{\vartheta\vartheta} (1)} - \beta_{\vartheta\vartheta} \tag{57}$$

These are consistent with the non-resonant conditions  $\lambda_1^F = 0$  (Eq 32) and  $\lambda_1^{FT} = 0$  (Eq 35), the latter with  $\alpha_{\vartheta\vartheta}(\Omega)$  approximated by  $\alpha_{\vartheta\vartheta} (1)$ . It is therefore confirmed the role of the coupling parameters  $\beta_{y\vartheta}$ ,  $\beta_{\vartheta\vartheta}$ , previously conjectured.

The eigenvectors  $(\hat{v}, \hat{\vartheta})^T = (a_1, a_2)^T$  at the critical conditions are evaluated from Eq (45); their expressions are reported in the Appendix C.

### 4.3 Discussion on perfect resonant galloping

The behavior of the system at the perfect resonance ( $\Omega = 1$ , i.e.  $\sigma = 0$ ) is discussed. Aim of the analysis is to investigate the effect of coupling on galloping. The task is to check if, and under which conditions, resonance reduces the uncoupled critical wind velocities (22)-(23), exerting a detrimental effect on the mechanical behavior.

According to Eq (51), the critical wind velocity at the resonance, viz.  $\mu = \mu_r$ , is the smallest root of the algebraic equation  $I_2(\mu) = 0$ . It is interesting to compare  $\mu_r$  to  $\mu_{min} := \min(\mu_y, \mu_{\vartheta} (1))$ , in order to find the conditions under which  $\mu_r < \mu_{min}$ . To this end, by making use of the definitions (22)-(23), the  $\alpha_{ij}$  and  $\beta_{ij}$  coefficients are rewritten as follows:

$$\begin{aligned} \alpha_{yy} &:= 2\xi_y \left(1 - \frac{\mu}{\mu_y}\right), & \alpha_{y\vartheta} &:= 2\frac{R}{b}\xi_y \frac{\mu}{\mu_y}, \\ \alpha_{\vartheta y} &:= \frac{2\xi_\vartheta}{R} \frac{\mu}{\mu_{\vartheta} (1)}, & \alpha_{\vartheta\vartheta} (1) &:= 2\xi_\vartheta \left(1 - \frac{\mu}{\mu_{\vartheta} (1)}\right) \\ \beta_{y\vartheta} &:= -2\frac{\mu^2}{\mu_y}\xi_y\delta, & \beta_{\vartheta\vartheta} &:= \frac{2\xi_\vartheta}{R} \frac{\mu^2}{\mu_{\vartheta} (1)} \end{aligned} \tag{58}$$

where:

$$\delta := \frac{|c'_t|}{|c'_t| - c_d} > 1 \tag{59}$$

and use has been made of Eqs (3). To simplify algebra, the usual hypothesis  $\frac{R}{b} = \frac{1}{2}$  (valid for compact sections) will be introduced from now on. With the previous expressions:

$$\begin{aligned} \operatorname{tr} \mathbf{A} &= 2(\xi_y + \xi_\vartheta) - 2\mu \left( \frac{\xi_y}{\mu_y} + \frac{\xi_\vartheta}{\mu_{\vartheta} (1)} \right) \\ \det \mathbf{A} &= 4\xi_y \xi_\vartheta \left[ 1 - \mu \left( \frac{1}{\mu_y} + \frac{1}{\mu_{\vartheta} (1)} \right) \right] \end{aligned} \tag{60}$$

A simpler case is considered first, in which  $\beta_{\vartheta\vartheta}$  is so small (as a consequence of  $c'_m$  being small) that it can be neglected. Accordingly,  $I_2(\mu) = 0$  brakes in two equations: (i)  $\operatorname{tr} \mathbf{A}(\mu) = 0$  and, (ii)  $\det \mathbf{A}(\mu) = 0$ . Since  $\operatorname{tr} \mathbf{A}(\mu) > 0$  in the interval  $(0, \mu_{min})$ , the smallest root is supplied by the vanishing of  $\det \mathbf{A}(\mu)$ , occurring at:

$$\mu_r^0 := \frac{\mu_y \mu_{\vartheta} (1)}{\mu_y + \mu_{\vartheta} (1)} < \min(\mu_y, \mu_{\vartheta} (1)) \tag{61}$$

It is concluded that, in the special (but frequent) case  $\beta_{\vartheta\vartheta} \simeq 0$ , the coupling decreases the critical load. This conclusion can be extended to the (frequent cases) in which  $\beta_{\vartheta\vartheta}$  is different from zero but it is small, for which it is expected that  $\mu_r$  is a small perturbation of  $\mu_r^0$ .

In the general case  $\beta_{\vartheta\vartheta} = O(1)$ , a closed form for  $\mu_r$  is no longer possible. However, it can be stated that  $\mu_r < \mu_{min}$ , when  $I_2(0)$  and  $I_2(\mu_{min})$  are opposite in sign (this being a sufficient, but not necessary condition, since an even number of roots could fall in the  $(0, \mu_{min})$  interval). Since,  $I_2(0) = \det \mathbf{A}(0) \operatorname{tr}^2 \mathbf{A}(0) > 0$ , this occurrence calls for  $I_2(\mu_{min}) < 0$ .

The different monomials in the expression (54) for  $I_2$  are considered: (i) since  $\det \mathbf{A}(\mu)$  decreases with  $\mu$  and vanishes at  $\mu_r < \mu_{min}$ , it is  $\det \mathbf{A}(\mu_{min}) < 0$ ; (ii) the second monomial is always negative; (iii) since either  $\alpha_{yy}$  or  $\alpha_{\vartheta\vartheta} (1)$  vanish at  $\mu_{min}$ , the last monomial vanishes. The key term, therefore, is the third one in Eq (54), in which, due to Eqs (58),  $\beta_{y\vartheta} > 0$ ,  $\alpha_{\vartheta y} > 0$ ,  $\beta_{y\vartheta} < 0$  for any  $\mu$ . Two cases must be examined, namely:



- if  $\mu_{min} = \mu_{\vartheta}(1)$ , it is  $\alpha_{yy}(\mu_{min}) > 0$ ,  $\alpha_{\vartheta\vartheta}(1; \mu_{min}) = 0$ , so that also the third term in  $I_2(\mu_{min})$  is negative; it is concluded, again, that  $\mu_r < \mu_{min}$ ;
- if  $\mu_{min} = \mu_y$ , it is  $\alpha_{yy}(\mu_{min}) = 0$ ,  $\alpha_{\vartheta\vartheta}(1; \mu_{min}) > 0$ , so that the third term in  $I_2(\mu_{min})$  is positive, calling for checking if it is larger or smaller than the sum of the moduli of the remaining terms.

It needs, therefore, to analyze the sign of  $I_2(\mu_y)$  when  $\mu_y < \mu_{\vartheta}$ . To this end, use is made of Eqs (58), to recast  $I_2(\mu_y)$  in the form:

$$I_2(\mu_y) = -16\xi_y\xi_{\vartheta}^2\frac{\mu_y}{\mu_{\vartheta}^3(1)} [4\xi_y\mu_{\vartheta}(1)\mu_y^3\delta^2 + \xi_{\vartheta}(\mu_{\vartheta}(1) - \mu_y)(\mu_{\vartheta}(1) - \mu_y - 4\mu_y^3\delta)] \tag{62}$$

An exact analysis of this expression is difficult. However, it can be strongly simplified if the following assumption is introduced, i.e.  $O(\mu_y^3) \gg O(\mu_y, \mu_{\vartheta}(1))$ , consistently with the initial guess  $O(\mu_y^2, \mu_{\vartheta}^2(1)) = 10$ . Therefore, by neglecting  $\mu_{\vartheta}(1)$  and  $\mu_y$  with respect  $4\mu_y^3\delta$ , it follows that:  $I_2(\mu_y) < 0$  when, either (a)  $\frac{\xi_y}{\xi_{\vartheta}}\delta > 1$ , or, (b):

$$\frac{\mu_{\vartheta}(1)}{\mu_y} < \frac{1}{1 - \frac{\xi_y}{\xi_{\vartheta}}\delta} \quad \text{when} \quad \frac{\xi_y}{\xi_{\vartheta}}\delta < 1 \tag{63}$$

The plane domain in Fig (3-a) resumes the results of this discussion. The shaded regions denote systems for which coupling is surely detrimental, i.e.  $\mu_r < \mu_{min}$ . The white region denotes system for which the resonant wind velocity is likely to be larger than  $\mu_{min}$ . This circumstance calls for: (i)  $\frac{\xi_y}{\xi_{\vartheta}}\delta < 1$ , (ii)  $\mu_{\vartheta}$  sufficiently larger than  $\mu_y$ , according to the inequality (63). Since  $\delta > 1$ , condition (i) is quite difficult to realize. By summarizing, the effect of coupling is almost everywhere detrimental in perfect resonance conditions.

Figure (3-b) shows the plot of  $I_2(\mu)$ (Eq (62), with no simplifications) in three cases: (A)  $\frac{\xi_y}{\xi_{\vartheta}}\delta > 1$ , (B)  $\frac{\xi_y}{\xi_{\vartheta}}\delta < 1$  and  $\frac{\mu_{\vartheta}(1)}{\mu_y}$  satisfying inequality (63), (C)  $\frac{\xi_y}{\xi_{\vartheta}}\delta < 1$  and  $\frac{\mu_{\vartheta}(1)}{\mu_y}$  violating inequality (63). The smaller intersection of the plot with the abscissa axis defines  $\mu_r$ , which is smaller than  $\mu_y$  in cases (A) and (B), and larger than  $\mu_y$  in case (C).

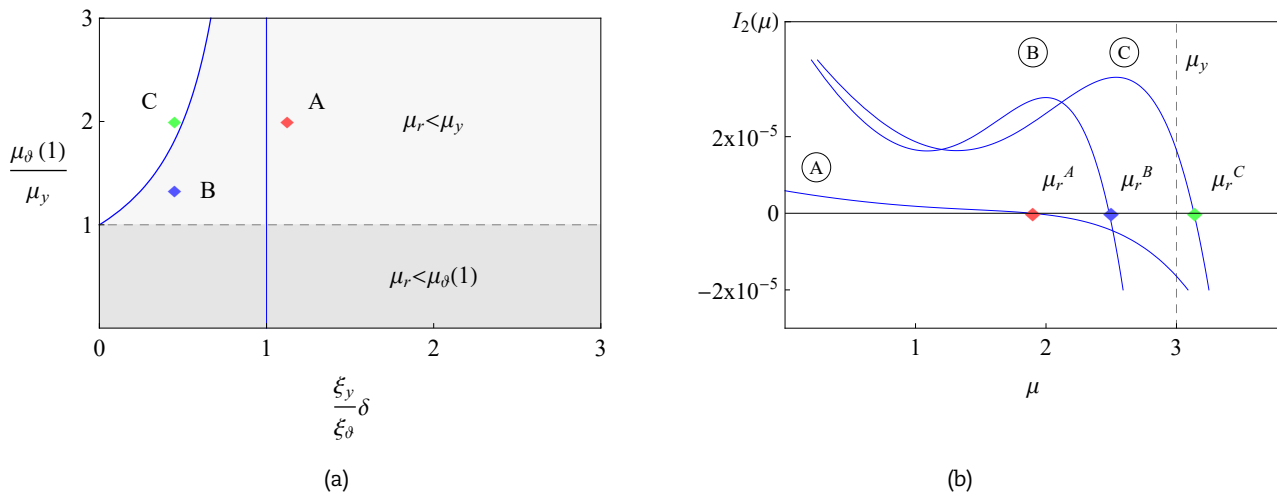


Figure 3. Analysis of the critical wind velocity  $\mu_r$  at the perfect resonance ( $\Omega = 1$ ): (a) plane parameter domain: shaded regions denote systems for which  $\mu_r < \min(\mu_y, \mu_{\vartheta}(1))$ ; (b) plots of  $I_2(\mu)$  for systems (A), (B), (C) marked in Fig (a), whose intersections with the abscissa axis define  $\mu_r$ ;  $\mu_y = 3$ ,  $\delta = 1.5$ ; (A)  $\mu_{\vartheta}(1) = 6$ ,  $\xi_y = 0.015$ ,  $\xi_{\vartheta} = 0.02$ , (B)  $\mu_{\vartheta}(1) = 4$ ,  $\xi_y = 0.015$ ,  $\xi_{\vartheta} = 0.05$ , (C)  $\mu_{\vartheta}(1) = 6$ ,  $\xi_y = 0.015$ ,  $\xi_{\vartheta} = 0.05$ .

### 5. Galloping of a tower building

To show how to apply the results of the proposed theory to a real prismatic structure, a sample problem is addressed, concerning the flexural-torsional galloping of a tower building, modeled as a homogeneous continuous. The mechanical properties of an equivalent cross-sectional model are first derived, and, in particular, the torsional-to-flexural frequency ratio is investigated over a range of geometrical parameters. Then, the aeroelastic stability of the discrete model is studied, for which exact and asymptotic solutions are implemented and compared.

#### 5.1 Continuous and sectional models

A multi-story tower building of height  $\ell$  is considered, consisting of  $n = \ell/h$  equal stories of height  $h$ , made of (assumed) infinitely rigid floors and elastic columns, arranged in a regular layout, respectful of the double symmetry (Fig (4)). The 3D discrete periodic system, according to [38, 39, 40], is modeled as a shear-shear-torsional 1D continuous beam, whose motion, transverse to the wind, is governed by (Fig 4-b):

$$\begin{aligned} GA^*V''(z, t) - m\ddot{V}(z, t) &= f_y^a(z, t) + f_y^d(z, t) \\ GJ\Theta''(z, t) - mr_C^2\ddot{\Theta}(z, t) &= c_z^a(z, t) + c_z^d(z, t) \\ V(0, t) = \Theta(0, t) = V'(\ell, t) = \Theta'(\ell, t) &= 0 \end{aligned} \tag{64}$$

Here:  $V(z, t)$  is the transverse displacement;  $\Theta(z, t)$  is the twist angle;  $GA^*$  the shear area;  $GJ$  the torsional stiffness;  $m$  the mass per unit length;  $r_C^2$  the squared inertia radius of the cross-section with respect its centroid  $G$ ;  $f_y^\alpha(z, t)$ ,  $c_z^\alpha(z, t)$  ( $\alpha = a, d$ ) are distributed aerodynamic and damping forces and couples; a dash denotes differentiation with respect the material coordinate  $z$ , and a dot with respect the time  $t$ .



Based on an energy equivalence (see, e.g., [38]), the mechanical properties of the continuous beam are linked as follows to those of the discrete system (see also [41], about the inclusion of shear walls in the model, and [42], for accounting for diagonal bracings):

$$GA^* = \frac{12}{h^2} \sum_{k=1}^N EI_{xk}, \quad GJ = \sum_{k=1}^N GJ_k + \frac{12}{h^2} \sum_{k=1}^N (EI_{xk} x_k^2 + EI_{yk} y_k^2) \tag{65}$$

$$m = \frac{\gamma_f A_f}{h}, \quad r_G^2 = r_{Gf}^2$$

where:  $EI_{xk}, EI_{yk}$  are the flexural stiffnesses of the  $k$ th column ( $k = 1, 2 \dots N$ ) with respect its principal inertia axes, assumed coincident with the coordinate axes;  $GJ_k$  is the torsional stiffness of the  $k$ th column;  $(x_k, y_k)$  are the coordinates of the intersection point of  $k$ th column with the floor, measured with respect to  $G$ ;  $A_f$  is the area of the floor and  $\gamma_f$  its surface mass density (the columns being assumed massless);  $r_{Gf}^2 = \frac{1}{A_f} \int_{A_f} (x^2 + y^2) dA$  is the squared inertia radius of the floor; moreover,  $f_y^a, c_z^a$  are the resultant forces, per unit length, of the aerodynamic pressures exerted by wind on the (supposed) continuous skin of the building; by referring to the quasi-steady theory [3] they are evaluated as:

$$f_y^a := \frac{1}{2} \rho_a U b [(c_d + c'_i) \dot{V} - R(c_d + c'_i) \dot{\Theta}] + \frac{1}{2} \rho_a U^2 b c'_i \Theta$$

$$c_z^a := \frac{1}{2} \rho_a U b [b c'_m \dot{V} - R b c'_m \dot{\Theta}] + \frac{1}{2} \rho_a U^2 b c'_m \Theta \tag{66}$$

with symbols previously defined. Finally, the damping forces will be introduced as modal components.

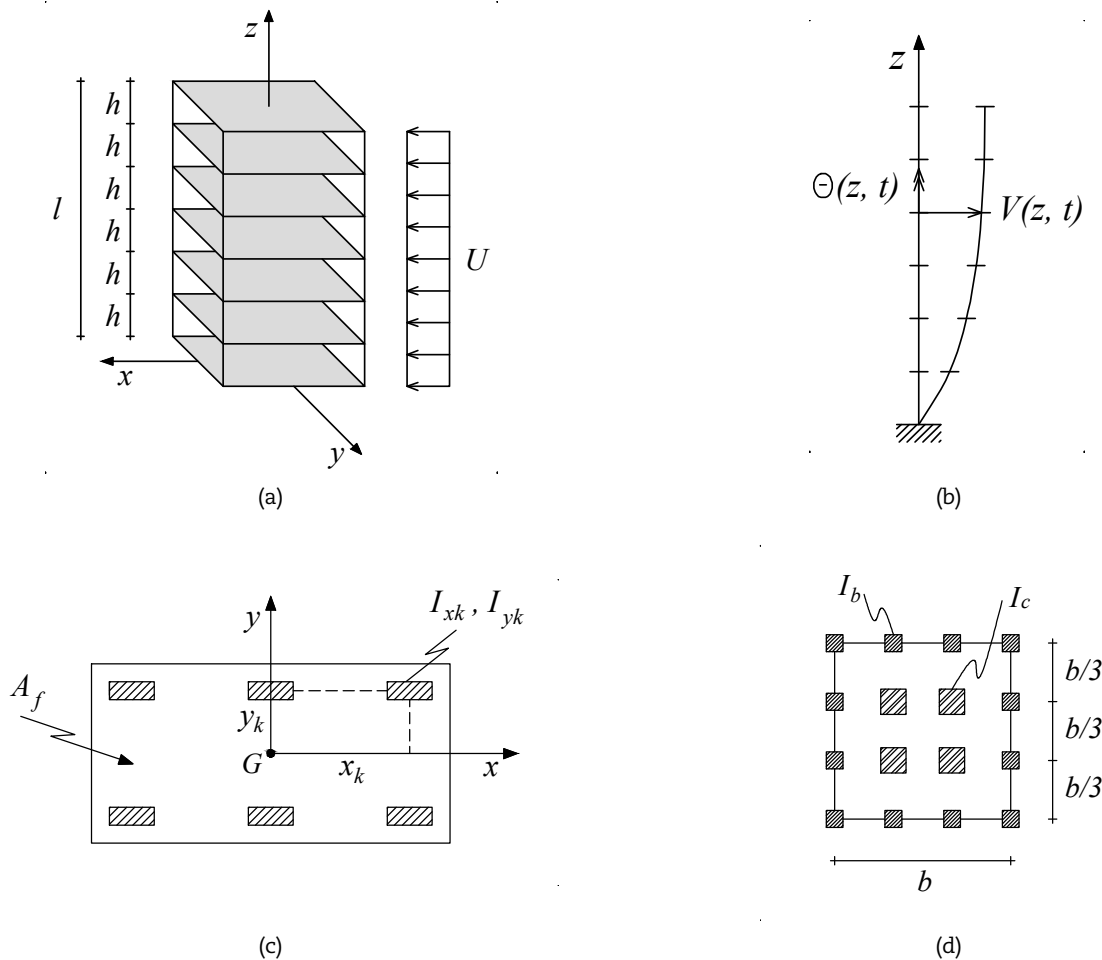


Figure 4. Tower building: (a) 3D view, (b) equivalent 1D beam, (c) generic column layout; (d) sample layout.

Equations (64), when the aerodynamic and damping forces are ignored, admit the exact fundamental natural frequencies:

$$\omega_y = \left(\frac{\pi}{2\ell}\right) \sqrt{\frac{GA^*}{m}}, \quad \omega_\Theta = \left(\frac{\pi}{2\ell}\right) \sqrt{\frac{GJ}{mr_G^2}} \tag{67}$$

It is worth noticing that the frequency ratio  $\Omega := \frac{\omega_\Theta}{\omega_y}$  is independent of length, as a consequence of having neglected the extension of the columns (which would call for a more complex Timoshenko beam model (see, e.g., [41])). Frequencies (67) are associated with the (uncoupled) natural modes:

$$\begin{pmatrix} \hat{V}(z) \\ \hat{\Theta}(z) \end{pmatrix} = \begin{pmatrix} 1 \\ 0 \end{pmatrix} \sin\left(\frac{\pi z}{2\ell}\right), \quad \begin{pmatrix} \hat{V}(z) \\ \hat{\Theta}(z) \end{pmatrix} = \begin{pmatrix} 0 \\ 1 \end{pmatrix} \sin\left(\frac{\pi z}{2\ell}\right) \tag{68}$$



By following the Galerkin approach, the beam is constrained to oscillated in its first flexural and torsional modes, i.e.:

$$V(z, t) = v(t) \sin\left(\frac{\pi z}{2\ell}\right), \quad \Theta(z, t) = \vartheta(t) \sin\left(\frac{\pi z}{2\ell}\right) \tag{69}$$

with  $v(t)$ ,  $\vartheta(t)$  Lagrangian parameters. The kinetic energy  $T$ , the elastic energy  $U$ , and the external work  $W$  spent by the forces (assumed constant in space) are computed as:

$$\begin{aligned} T &= \frac{1}{2} \int_0^\ell m \dot{V}^2(z, t) dz + \frac{1}{2} \int_0^\ell m r_G^2 \dot{\Theta}^2(z, t) dz = \frac{1}{2} m \frac{\ell}{2} \dot{v}^2(t) + \frac{1}{2} m r_G^2 \frac{\ell}{2} \dot{\vartheta}^2(t) \\ U &= \frac{1}{2} \int_0^\ell G A^* V'^2(z, t) dz + \frac{1}{2} \int_0^\ell G J \Theta'^2(z, t) dz = \frac{1}{2} G A^* \frac{\pi^2}{8\ell} v^2(t) + \frac{1}{2} G J \frac{\pi^2}{8\ell} \vartheta^2(t) \\ W &= \int_0^\ell f_y V(z, t) dz + \int_0^\ell c_z \Theta(z, t) dz = \frac{2}{\pi} f_y \ell v(t) + \frac{2}{\pi} c_z \ell \vartheta(t) \end{aligned} \tag{70}$$

By equating these energies/work to those of the two degree-of-freedom system, the modal masses  $M, \mathcal{J}_G$ , the modal stiffnesses  $K_y, K_\vartheta$  and the modal forces/couples  $F_y, C_z$ , are evaluated as:

$$M := m \frac{\ell}{2}, \quad \mathcal{J}_G := M r_G^2 \tag{71}$$

$$K_y := \frac{\pi^2}{8} \frac{G A^*}{\ell}, \quad K_\vartheta := \frac{\pi^2}{8} \frac{G J}{\ell} \tag{72}$$

$$F_y = \frac{2}{\pi} f_y \ell, \quad C_z = \frac{2}{\pi} c_z \ell \tag{73}$$

Equations (71),(72) supply the inertial and stiffness parameters appearing in the discrete model, Eqs (2). When Eqs (73) are compared with the resultant of forces acting on a rigid cylinder of length  $L$ , i.e.  $F_y = f_y L, C_z = c_z L$ , its length is identified as  $L = \frac{2\ell}{\pi}$ .

### 5.2 Frequency analysis of a family of tower buildings

A family of tower buildings of squared cross-section of side  $b$  is considered. The column layout consists of four rows of four equispaced columns, all having squared cross-sections. Columns at the boundary, however, have geometrical characteristics  $E I_b, G J_b$  different from those of the four central columns,  $E I_c, G J_c$ . The elastic properties (65), when specialized to the case at hand, read:

$$\begin{aligned} G A^* &= \frac{12}{h^2} E I_b (12 + 4\chi) \\ G J &= G J_b (12 + 4\chi) + \frac{8}{3} \left(\frac{b}{h}\right)^2 E I_b (19 + \chi) \end{aligned} \tag{74}$$

where  $\chi := \frac{E I_c}{E I_b} = \frac{G J_c}{G J_b}$  is a stiffness ratio. The inertial properties (65) are:

$$m = \frac{\gamma_f b^2}{h}, \quad r_G^2 = \frac{b^2}{6} \tag{75}$$

By substituting Eqs (74), (75) in the modal quantities (71)-(72), the parameters of the sectional model are evaluated. In particular, the frequency ratio  $\Omega = \sqrt{\frac{G J}{G A^* r_G^2}}$  reads:

$$\Omega = \sqrt{\frac{1}{2} \frac{G J_b}{E I_b} \left(\frac{h}{b}\right)^2 + \frac{1}{3} \left(\frac{19 + \chi}{3 + \chi}\right)} \tag{76}$$

Since, for a squared cross-section of side  $a$ , it is  $J_b \simeq 0.141 a^4, I_b = \frac{1}{12} a^4$ , by assuming  $G = 0.4E$ , it results that  $\frac{G J_b}{E I_b} = 0.677$ . In Fig 5 the frequency ratio is plotted *vs* the parameter  $\chi$  for two values of the  $\frac{h}{b}$  geometrical ratio. It is seen that the torsional stiffness of the columns is negligible with respect the flexural one. When  $\chi$  is varied, the frequency ratio crosses the resonance value  $\Omega = 1$ , at  $\chi = \chi_r \simeq 5$ . When  $\chi < \chi_r$  the lower frequency is of flexural type; when  $\chi > \chi_r$  the lower frequency is of torsional type. For example: if the columns are all equal ( $\chi = 1$ ), it is  $\Omega \simeq 1.29$ ; if the central columns have side double of that at the boundary, it is  $\chi = 16$ , and therefore,  $\Omega \simeq 0.78$ . When  $\chi \rightarrow \infty$ , then  $\Omega \rightarrow 0.577$ . The example shows that both ranges  $\Omega < 1$  and  $\Omega > 1$  are worth of being investigated.

### 5.3 Galloping analysis of a sample building

Referring to the family systems in Fig. (4-d), a sample building is considered, characterized by the following dimensional characteristics:  $b = 15$  m,  $m \simeq 10^5$  kg/m,  $r_G^2 \simeq 37.5$  m<sup>2</sup>, considering  $\rho_a = 1.25$  kg/m<sup>3</sup>. Therefore, the relevant dimensionless parameters become:  $\eta_y = 0.0014, \eta_\vartheta = 0.0084$ . The aerodynamic coefficients are taken as [14]:  $c_d = 2.04, c'_l = -4.381, c'_m = 0.496$ ; moreover, the following modal damping ratios are set:  $\xi_y = 0.0080, \xi_\vartheta = 0.0089$ . According to Eqs (4):  $\alpha_{yy} := 0.16 - 0.0032774\mu, \alpha_{y\vartheta} := 0.0016387\mu, \alpha_{\vartheta y} := 0.0041664\mu, \alpha_{\vartheta\vartheta}(\Omega) := 0.0178\Omega - 0.0020832\mu, \beta_{y\vartheta} := -0.0061334\mu^2, \beta_{\vartheta\vartheta} := 0.0041664\mu^2$ . From Eqs (22)-(23),  $\mu_y := 4.88192$  (corresponding to a reduced wind speed greater than 30) and  $\mu_\vartheta(\Omega) := 8.54455\Omega$  follow, so that  $\mu_\vartheta(\Omega) < \mu_y$ , when  $\Omega < 0.571349$  and  $\mu_\vartheta(\Omega) > \mu_y$ , when  $\Omega > 0.571349$ , with  $\Omega$  given by Eq (76). For the sake of simplicity, the mean wind speed  $U$  is not considered variable along the height of the building but it is representative of the wind velocity at a suitable height of the building (e.g., 0.8ℓ), as usual in technical papers on aeroelastic phenomena (e.g., [43]).



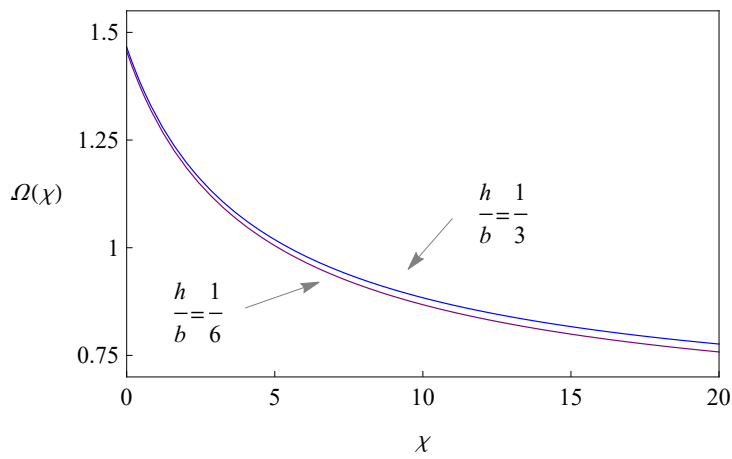


Figure 5. Frequency ratio of the tower building  $\Omega$  vs the stiffness ratio parameter  $\chi$  (story height  $h$ , cross-section side  $b$ ).

### 5.3.1 Linear stability analysis

An exact galloping analysis is first carried out along the lines discussed in Sect 3. The numerical solution of the fifth-degree characteristic equation (13) leads to the linear stability diagram of Fig. (6-a), plotted on the bifurcation parameter plane  $(\Omega, \mu)$ . Up to three real and positive solutions  $\Omega(\mu)$  are found. Four branches are recognized: branches (I,II) are of flexural (F) type (as it will appear clear from the eigenvector analysis); branches (III,IV) are of flexural-torsional (FT) type. The branches mutually cross at two points,  $DH_1 = (0.3578, 4.1730)$ ,  $DH_2 = (1.4199, 7.6995)$ , denoting the occurrence of double Hopf bifurcations, according to the findings of Sect 3.2 (in particular, Eq (21)). The shaded region in the parameter plane denotes stable systems, the remaining part unstable systems. When, for a fixed  $\Omega$ , the distinguished wind parameter  $\mu$  is increased from zero, the system loses stability at a critical value which depends on  $\Omega$ . By monotonically increasing  $\Omega$ , galloping manifests in sequence as FT, F, FT and again F type. The critical wind velocity is lower than the Den Hartog velocity  $\mu_y$  until  $\Omega$  is slightly bigger than 1 (about 1.1 in Fig. 6-a), reaching the minimum value  $\mu_r$  close to the resonance; then it becomes greater than  $\mu_y$  with maximum value at  $DH_2$  point, where it reaches an increase of about 50% compared to  $\mu_y$ , highlighting a remarkable beneficial effect due to the modal interaction. Finally, the critical wind velocity decreases asymptotically (from above) to the Den Hartog critical speed  $\mu_y$  for large  $\Omega$  (greater than 2); moreover, it is almost everywhere lower than  $\mu_\vartheta(\Omega)$ , except for small  $\Omega$ 's, where it is slightly higher. This results is in agreement with the analysis developed in Sect 4.3, relevant to the perfect resonance  $\Omega = 1$ , since  $\frac{\xi_y}{\xi_\vartheta} \delta = 1.68218 > 1$  (see Fig. (3)). On the whole, the scenario fully agrees with the qualitative one envisaged by Fig. (2), predicted for small and large  $\Omega$ 's via asymptotic analysis.

Figure (6-b) reports the Hopf frequency  $\omega$  (i.e. the imaginary part of the critical eigenvalue) at the incipient bifurcation, according to Eq (12). It is seen that: (i) when galloping is of flexural type (branches I,II) it is  $\omega = 1$ , i.e. periodic oscillations arise at the nondimensional flexural frequency (to be corrected by nonlinearities as a function of the amplitude); (ii) when galloping is of flexural-torsional type, the Hopf frequency is equal to the nondimensional torsional frequency  $\Omega$  along branch IV (large  $\Omega$ ) but remarkably differs from it along branch III (small  $\Omega$ ). Figures (6-c,d) are enlargements of the previous sub-figures (6-a,b), explaining the transition from the different branches in order to the better depict the situation in the neighborhood of the resonance condition. The gap between branches I and II in Fig. (6-b) is due to the fact that only branches III and IV exist in this interval of  $\mu$ , on the boundary of the stability domain, Fig. (6-a).

The previous analysis is repeated by using perturbation expansions, in order to check the reliability of the analytical solutions. First, the non-resonant asymptotic solution (Sect 4.1) is employed, leading to the results displayed in Fig (7). Figure (7-a) shows the linear stability diagram. Here, the (green) branches I,II denote incipient instability via a flexural mode, as described by the explicit Eq (37); the (green) branches III, IV are loci of incipient instability of flexural-torsional type, as determined by solving the cubic equation (38). The associated Hopf frequencies are shown in Fig. (7-b): they are provided by the imaginary part of the  $\lambda_0$  eigenvalue, as given by Eqs (29) and (30), respectively. Both figures report, for comparison, the exact solution of Fig. (6-a,b) (light red markers). As a general comment, it was found that the non-resonant asymptotic solutions provide an excellent approximation of the exact solution, except for a narrow interval around the perfect resonance,  $\Omega = 1$ , where they predict wrong results.

Close to  $\Omega = 1$ , the resonant solution obtained in Sect 4.2 must be used. By solving the second-degree Eq (51), the linear stability diagram of Fig. (8-a) is obtained. A suitable enlargement (Fig. 8-b) shows that the resonant solution accurately describes the smooth transition from the (F) branch I to the (FT) branch IV, capturing the strong reduction of the critical wind velocity: however, it also gives a reasonably good approximation of the exact solution for  $\Omega$  sufficiently greater than 0 (Fig. 8-a), since the larger errors concern bifurcations higher than the first one. Finally, concerning the Hopf frequency, Fig. (8-c) confirms an excellent precision of the resonant perturbation solution for  $\Omega \simeq 1$ .

To analyze possible different effects due to the presence of torsion, the damping ratios of the sample systems are modified into  $\xi_y = 0.015, \xi_\vartheta = 0.050$ , then  $\frac{\xi_y}{\xi_\vartheta} \delta = 0.5614 < 1$ , while leaving the mass ratios unchanged; the critical wind velocities become  $\mu_y = 9.1536, \mu_\vartheta(\Omega) = 48.0031\Omega$ , so that, at the perfect resonance,  $\frac{\mu_\vartheta(1)}{\mu_y} = 5.2441$ , violating the inequality (63). The relevant linear stability diagram of Fig. (6-a) changes into that of Fig. (9), which shows a possible beneficial effect of the interaction also in perfect resonant conditions, being  $\mu_r = \mu(1) > \mu_y$ . This diagram shows the excellent agreement of the resonant and non resonant perturbation solutions with the exact one in the whole  $\Omega$  interval, also in this particular case. Moreover, the branch IV here rises towards the vertical asymptote  $\Omega = 1$  and the branch II lowers, so that there is no more intersection between these two branches. Figure (9) clearly shows that, if  $\Omega$  is quasi-statically increased, the stability diagram falls from point  $P_1$ , on branch IV, to point  $P_2$ , on branch II, with a sudden, noticeable decrease in the critical wind velocity.

Finally, a discussion on the role of the  $\beta_{ij}$  parameters (mainly  $\beta_{y\vartheta}$ ), namely on the error could be committed by neglecting them, is carried out. A measure of the error committed by neglecting both  $\beta_{ij}$  parameters is displayed in Table 1, where the exact and approximate values of the critical wind velocity, and their relative errors, have been evaluated for different  $\Omega$ 's ratios. The numerical values show that, far away from the resonance (e.g.,  $\Omega = 0.5, 2$ , on flexural branches), the  $\beta_{ij}$  parameters have a small influence on the critical wind velocity, while, close to the resonance ( $\Omega = 1$ ) or even quite far from it (e.g.,  $\Omega = 1.3, 1.5$ , on both



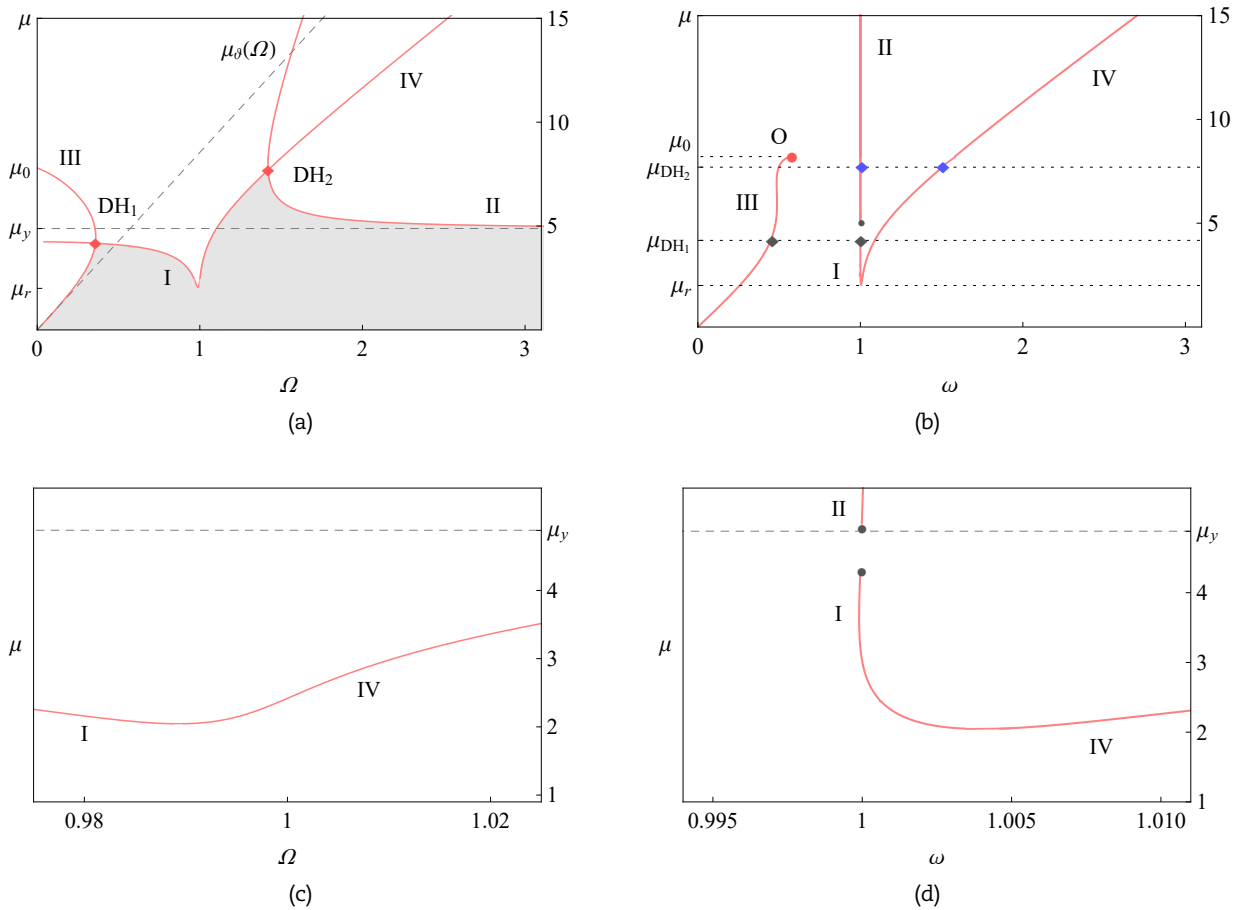


Figure 6. Exact galloping analysis of the sample system: (a) linear stability diagram in the bifurcation parameter plane  $(\Omega, \mu)$ ; (b) Hopf frequency  $\omega$  vs  $\mu$ ; (c,d) enlargements of the resonant region,  $\Omega \simeq 1$ . (I,II) flexural branches, (III,IV) flexural-torsional branches.

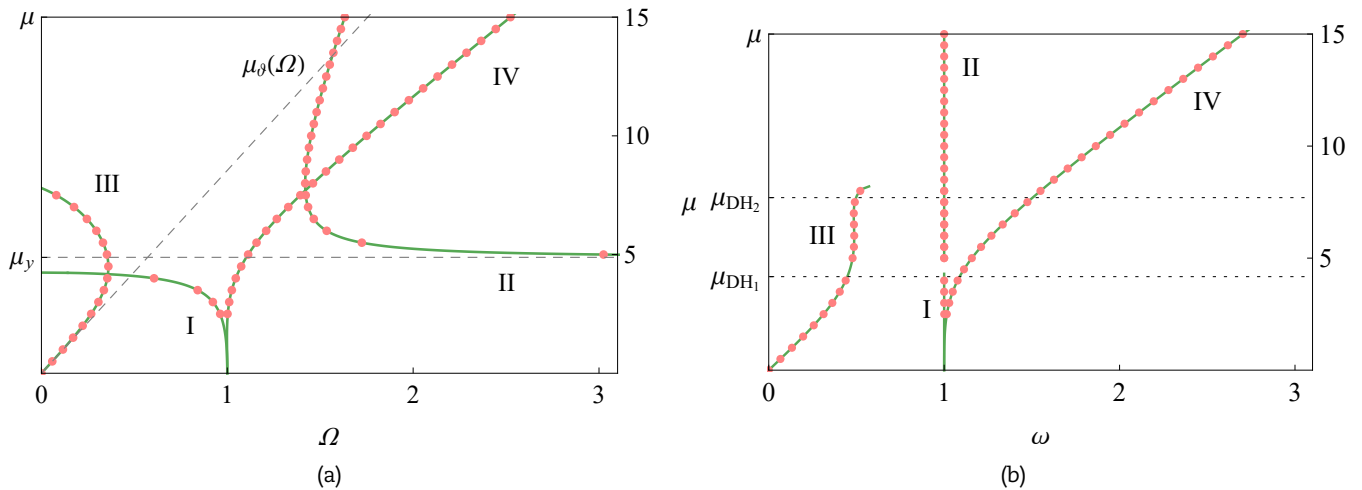


Figure 7. Non-resonant perturbation solutions: (a) linear stability diagram, (b) Hopf frequency. Flexural branches (green I,II lines), flexural-torsional branches (green III,IV lines) vs exact solution (light red markers).

flexural-torsional and flexural branches), they strongly affect it. This is due to the role that the  $\beta_{ij}$  parameters exert on the coupling between the two DOFs. Therefore, the  $\beta_{ij}$  parameters are important in a large  $\Omega$  range containing the resonant condition.

### 5.3.2 Critical modes

The analysis of the modes in critical conditions is then carried out. Figure (10) shows the real and imaginary parts of the torsional component  $\hat{\vartheta}$  of the critical eigenvector, as evaluated by the exact solution, Eq (14), having put  $\hat{\nu} = 1$ . The perturbation results are also reported, in terms of both non resonant solutions (green lines), Eqs (29), (33) and (30), (36) for F and FT modes respectively, and resonant solutions (black lines), Eqs 44 and Appendix C. The analysis of critical eigenvectors versus  $\Omega$  confirms the F or FT character of the associated branches in Fig. (6). The agreement of the non resonant perturbation solutions with the exact solution is excellent except for a small interval around the resonance; the resonant perturbation solution perfectly matches with the exact solution when  $\Omega \simeq 1$ , as highlighted by the enlargements of the resonance region, Figure (10-c,d). Moreover, Figure (10-e,f) shows



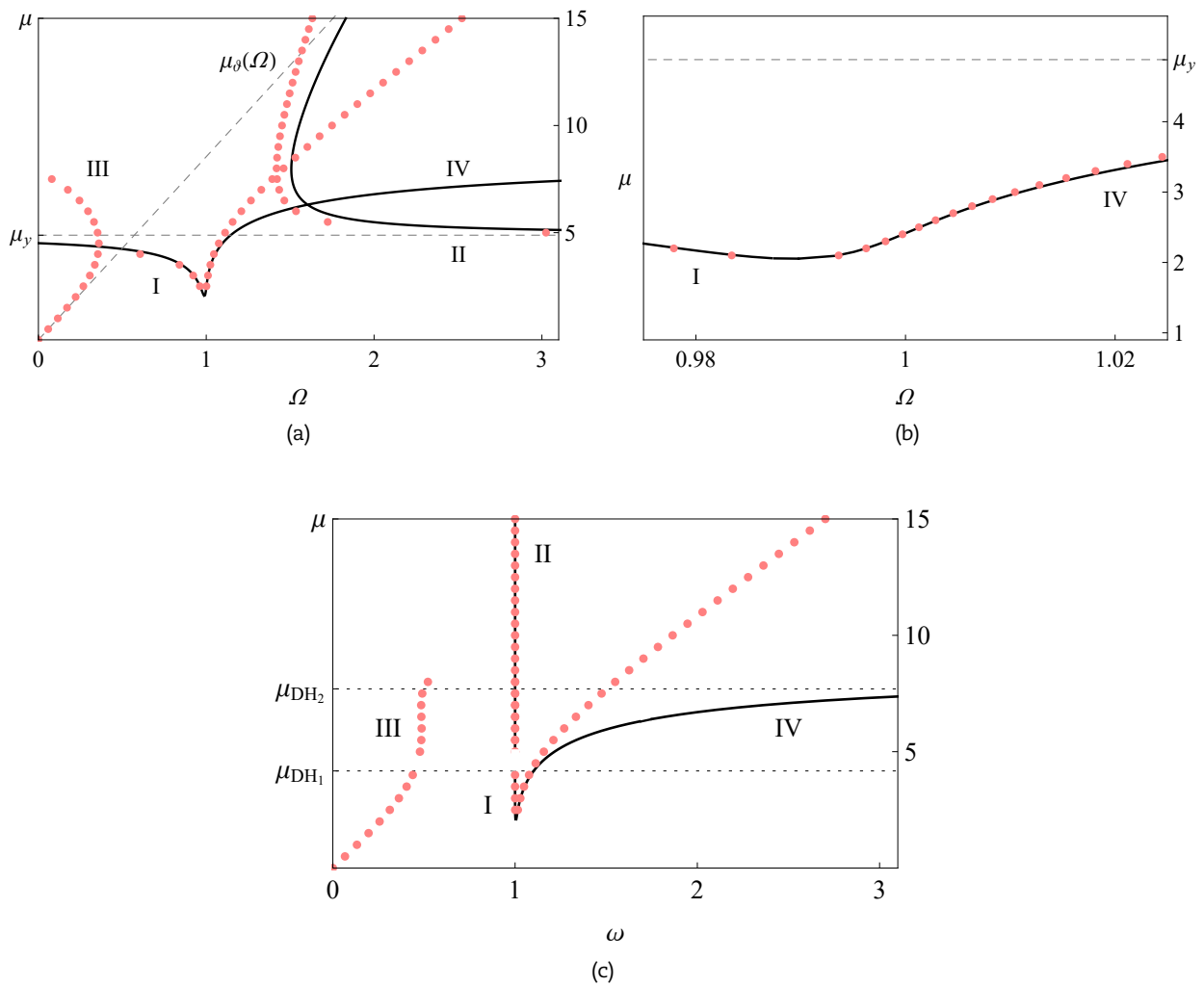


Figure 8. Resonant perturbation solutions: (a) linear stability diagram in the bifurcation parameter plane ( $\Omega, \mu$ ); (b) enlargements of the resonant region  $\Omega \simeq 1$ ; (c) Hopf frequency  $\omega$  vs  $\mu$ . Perturbation resonant solutions (black lines) vs exact solution (light red markers).

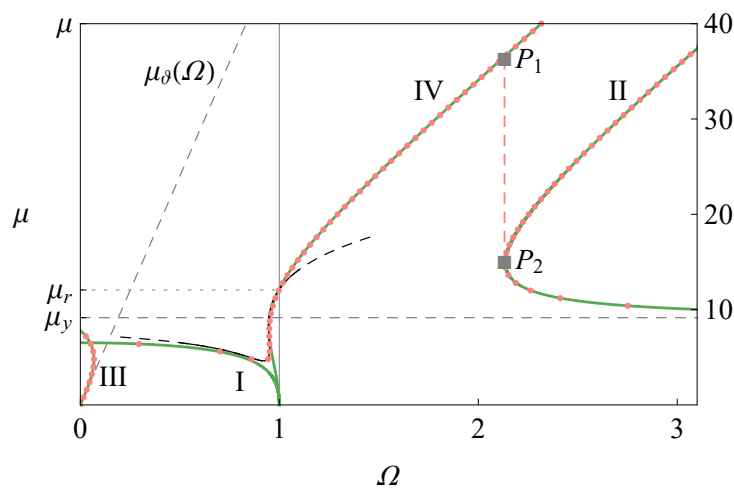


Figure 9. Linear stability diagram for the modified sample system ( $\xi_y = 0.015, \xi_{\vartheta} = 0.050$ ). Perturbation resonant (black thin lines) and non resonant (green thick lines) solutions vs exact solution (light red markers).

the analysis of critical modes in terms of magnitude and phase angle of the (complex) torsional component  $\hat{\vartheta}$ , in order to highlight the relative phase between flexure and torsion. For the sake of simplicity, these last two figures are carried out through the only exact solution (light red thin lines), which is in excellent agreement with the perturbation solutions, as shown above. It can be noted that the phase angles of the critical modes are approximately piece-wise constant as  $\Omega$  varies, with the exception of the resonance zone. Flexural branches I e II have a phase angle of approximately  $\pm \frac{\pi}{2}$ , respectively, since the torsional component is nearly pure imaginary and very small in these cases, except in the vicinity of the resonance. Flexural-torsional branches III e IV have an argument approximately equal to 0 and  $-\pi$ , respectively, since the torsion is almost real for these critical conditions.

Figure (10) points out that the critical modes are generally complex in nature because of the aerodynamic coupling of the system



Table 1. Influence of the  $\beta_{ij}$  parameters on the critical wind velocity as  $\Omega$  varies.

$\Omega$	Branch	$\mu (\beta_{ij} \neq 0)$	$\mu (\beta_{ij} = 0)$	% relative error
0.5	I	4.0947	4.2722	4.3
1	I	2.4182	3.1068	28.5
1.2	IV	5.9155	4.879	-17.5
1.3	IV	6.7761	4.8805	-28
1.5	II	6.1980	4.8813	-21.2
2	II	5.2425	4.8817	-6.9
2.5	II	5.0710	4.8818	-3.7

under investigation, which presents a full damping matrix due to the fluid-structure interaction terms. The modal interaction in resonance appears evident from the arising of a significant real part of torsional type. The imaginary component is present in a limited way in the F modes away from resonance, while it becomes significant close to the resonance and characterizes all FT modes as a whole, even though it is much smaller than the corresponding real component.

Limited to non resonant conditions, few sample elliptical trajectories, each relevant to the different branches (from I to IV) executed by the system on the border of stability, are presented in Fig. (11) using the exact solution, Eq (15). It appears that the 'degree of complexity', denoted by the minor-to-major semi-axis length ratio, is however very limited in all these cases, and it is definitely larger when the mode is of FT-type (branches III and IV). The enlargement in the figure shows the shape of F-type branches by means of a strongly deformed scale on the ordinate axis. The trajectories deriving from the perturbation solutions are nearly coincident with those depicted by the exact solution; therefore, they have not been reported here for the sake of simplicity.

Moving on to analyze the behaviour near the resonant region, Fig. (12) presents the eigensolutions resulting from the application of the exact solution on the critical border. Fig. (12-a) shows the real part of the two eigenvalues while Fig. (12-b) shows the corresponding imaginary part. The critical eigenvalue (red line) has an initially unitary imaginary part (F-type branch) that undergoes a sharp upward bend when it approaches the imaginary part of the stable eigenvalue (green line), near the condition of perfect resonance ( $\Omega \simeq 1$ ). At the same time the stable eigenvalue undergoes an opposite trend, passing from an imaginary part less than 1, typical of FT-type branches, to a unitary imaginary part approaching the resonance. This hybridization between a critical and a stable mode recalls the *veering* of conservative systems (e.g., [44]) which, however, occurs between two (marginally) stable modes. This phenomenon has also been observed in aeroelastic problems (e.g., [45]) when wind speed is varying, close to the critical condition; here it is instead presented on the shape evolution of the eigensolutions relative to the first critical condition of the system, as the frequency ratio  $\Omega$  varies. Veering can also be effectively observed on trajectories. Fig. (12-c) shows the trajectories of the critical eigenvectors around the resonance, while Fig. (12-d) points out those of the stable eigenvectors, which are stable spirals, having the corresponding eigenvalues real negative part, Fig. (12-a). The critical trajectories start from a F-type behavior and, turning counterclockwise, are transformed into FT-type as  $\Omega$  increases; at the same time, in an opposite way, the stable trajectories start from a type FT-type behavior to become F-type reaching the resonance. The 'degree of complexity' of the modes, which is very modest outside the resonance, as seen in Fig. (11), becomes much more relevant in these resonant cases.

## 6. Conclusions

A linear stability analysis of prismatic structures, possessing two planes of symmetry and undergoing galloping, has been carried out. A two degree-of-freedom model has been implemented, accounting for cross-wind translation and rotation of the cross-section. They describe, in a Galerkin perspective (or in an equivalent sectional model approach), the flexural and torsional behavior of the cylinder. By using the quasi-steady assumption for the aerodynamic forces, a set of two coupled ordinary differential equations has been derived.

An exact analysis has first been carried out, calling for numerical solutions of polynomial equations describing the eigensolution of the system under investigation. The analysis revealed the possible existence of double Hopf bifurcation points, at which two galloping modes manifest simultaneously. Then, an asymptotic analysis has been developed, both (i) far and (ii) close to the resonance. The analysis provided either (i) closed-form formulas for critical velocity, Hopf frequency and eigenvectors or, (ii) implicit formulas of lower-degree with respect the exact ones. Moreover, it allowed for drawing qualitative information on stability for small and large flexural-to-torsional frequency ratios. More remarkably, the asymptotic analysis furnished a sufficient criterion to establish under which conditions, close to the resonance, the critical load of the coupled system is lower than the critical load of the one degree-of-freedom systems in which coupling is ignored.

As an application, a tower building has been considered, modeled as an equivalent shear-torsional beam. It has been shown that, by varying the stiffnesses of the columns, the frequency ratio spans an interval containing the unitary resonant value. A sample system has been considered, by using the frequency ratio as a parameter. For it, the following conclusions are drawn.

1. The boundary of the stability diagram in the wind-frequency ratio plane is made of flexural-torsional and flexural branches, which alternate each other, separated by two double Hopf bifurcation points.
2. The critical wind velocity is smaller than the two uncoupled critical velocities for a significant interval of the  $\Omega$ -axis, usually for values sufficiently greater than zero and slightly larger than one. Outside of this interval, the beneficial effects on the critical wind velocity, due to the modal interaction, prevail. This behavior typically occurs for  $\Omega$  sufficiently greater than 1, but, in particular conditions, it can also propagate at perfect resonance. At the Double Hopf bifurcation  $DH_2$ , for  $\Omega \simeq 1.42$  in the example presented above, the critical velocity is considerably greater (e.g., +50%) than that of pure plunge, ruled by the classic Den Hartog criterion.
3. Flexural motion at bifurcation occurs at the flexural frequency; flexural torsional motions at a frequency which depends on both the structural frequencies.
4. Modes are generally complex, so that the system travels elliptical trajectories in the plane of the configuration variables. Their 'degree of complexity' is very small in non-resonance cases (i.e., the ellipses are very flattened) while it becomes more significant around the resonant condition.



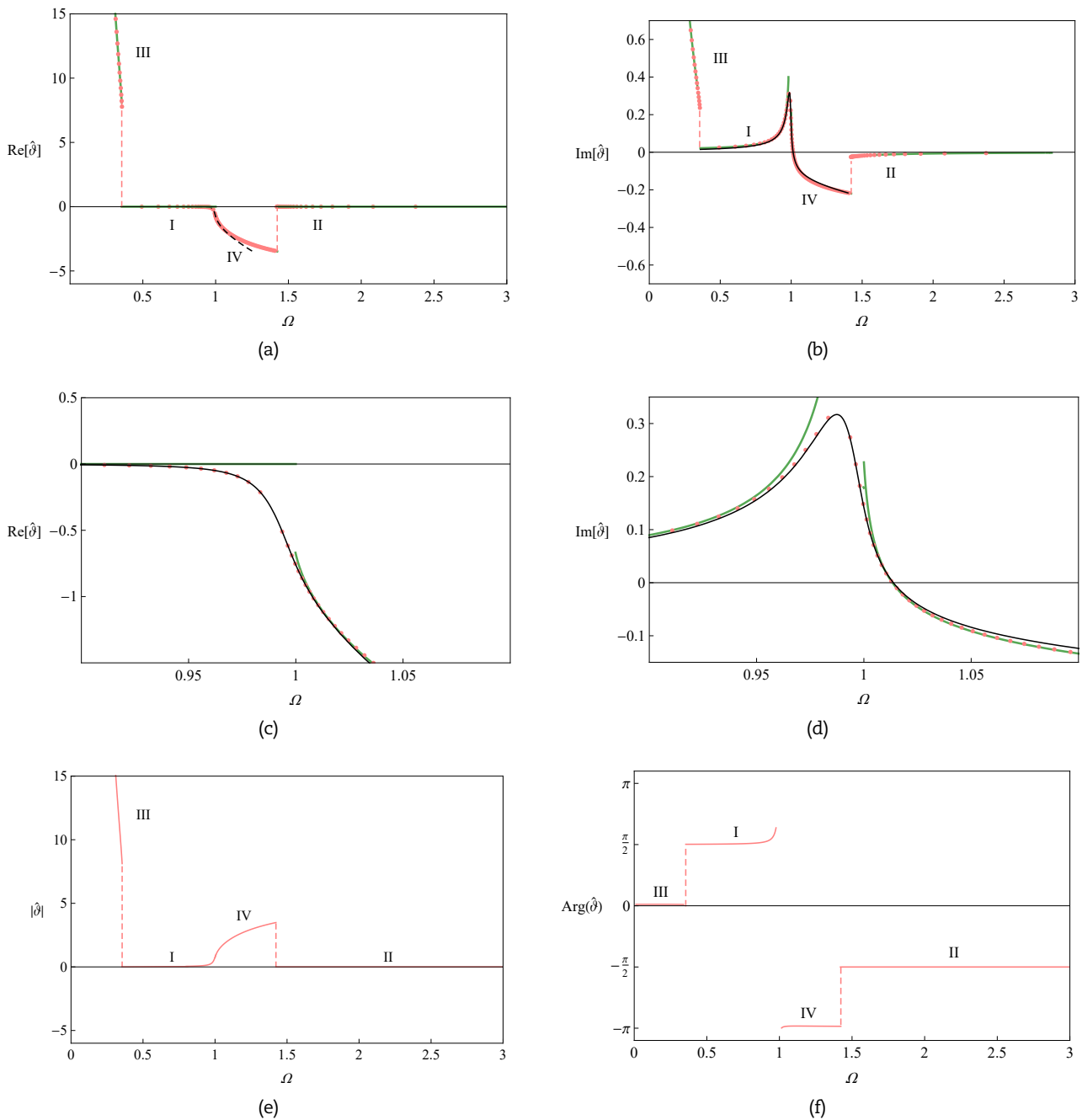


Figure 10. Galloping critical mode analysis: (a) real and (b) imaginary of the torsional component  $\hat{\vartheta}$  vs  $\Omega$ ; (c,d) enlargements of the previous diagram around the resonant region,  $\Omega \simeq 1$ ; (e) magnitude and (f) argument of the torsional component  $\hat{\vartheta}$  vs  $\Omega$ . Perturbation resonant solution (black thin lines), perturbation non resonant solution (green thick lines), exact solution (light red markers in a-d, light red thin lines in e-f).  $\dot{\vartheta} = 1$  was taken as normalization.

5. Close to the resonance, a veering phenomenon occurs with a hybridization between a critical and a stable mode: the critical mode changes its nature from flexural to flexural-torsional type.
6. The asymptotic analysis is in excellent agreement with exact results. The non-resonant solution provides very good results everywhere, except in a narrow interval close to the resonance; the resonant solution accurately captures the solution in this interval, and supplies reasonably approximated results far from resonance. As a whole, the asymptotic approach allows to correctly describe the global scenario from a qualitative point of view.

As a further theoretical research to be developed on this topic, the study of the nonlinear behavior of the system, beyond the loss of linear stability, is of great importance. Moreover, the nonlinear analysis of the double Hopf bifurcation is believed to supply a key for an understanding of the complex interaction phenomenon. All the nonlinear analysis can be carried out via perturbation analysis, along the lines of, e.g., [31, 32, 35].

### Author Contributions

All authors contributed equally to this work. Angelo Luongo and Giuseppe Piccardo conceived the scientific idea of this paper. Angelo Luongo developed analytical solutions and Francesca Pancella carried out numerical simulations. The manuscript was



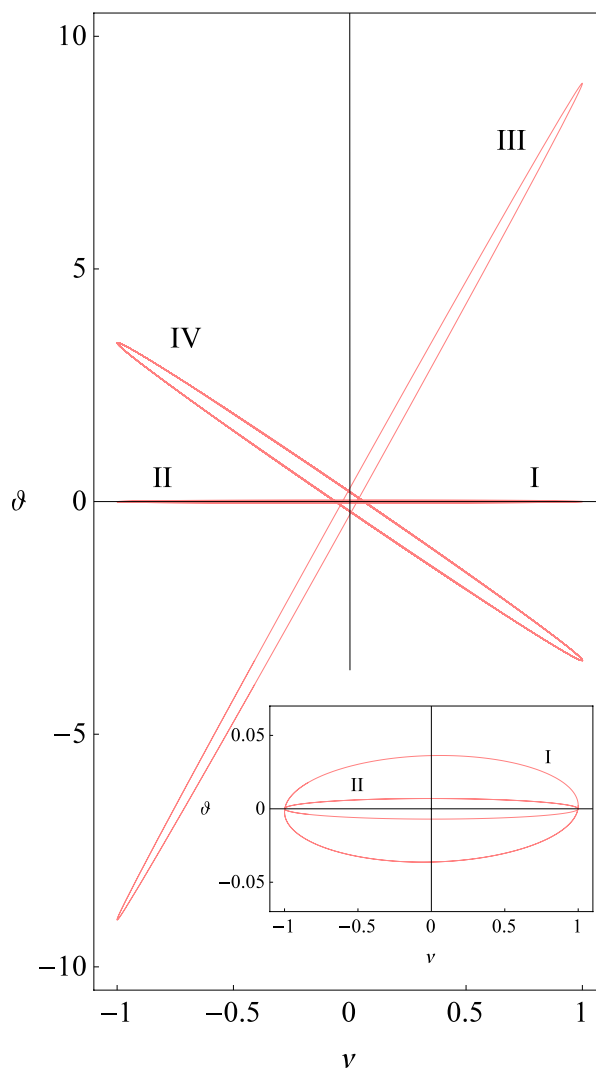


Figure 11. Trajectories of critical modes in the  $(v, \vartheta)$  plane for non resonant cases :  $\Omega = 0.35$  (III),  $0.7$  (I),  $1.4$  (IV),  $2$  (II).

written through the contribution of all authors. All authors discussed the results, reviewed and approved the final version of the manuscript.

### Conflict of Interest

The authors declared no potential conflicts of interest with respect to the research, authorship and publication of this article.

### Funding

The authors received no financial support for the research, authorship and publication of this article.

### References

- [1] Den Hartog, J., *Mechanical Vibrations*, Dover Publications, 1985.
- [2] 207/2018, C.D.R., *Guide for the assessment of wind actions and effects on structures*, National Research Council of Italy, Rome, Italy, 2020.
- [3] Piccardo, G., Pagnini, L., Tubino, F., Some research perspectives in galloping phenomena: critical conditions and post-critical behavior, *Continuum Mechanics and Thermodynamics*, 2015, 27, 261–285.
- [4] Blevins, R., *Flow-induced Vibration*, Krieger Publishing Company, Florida, 2nd ed., 2001.
- [5] Solari, G., Pagnini, L., Gust buffeting and aeroelastic behaviour of poles and monotubular towers, *Journal of Fluids and Structures*, 1999, 13(7-8), 877–905.
- [6] Pagnini, L., Piccardo, G., A generalized gust factor technique for evaluating the wind-induced response of aeroelastic structures sensitive to vortex-induced vibrations, *Journal of Fluids and Structures*, 2017, 70, 181–200.



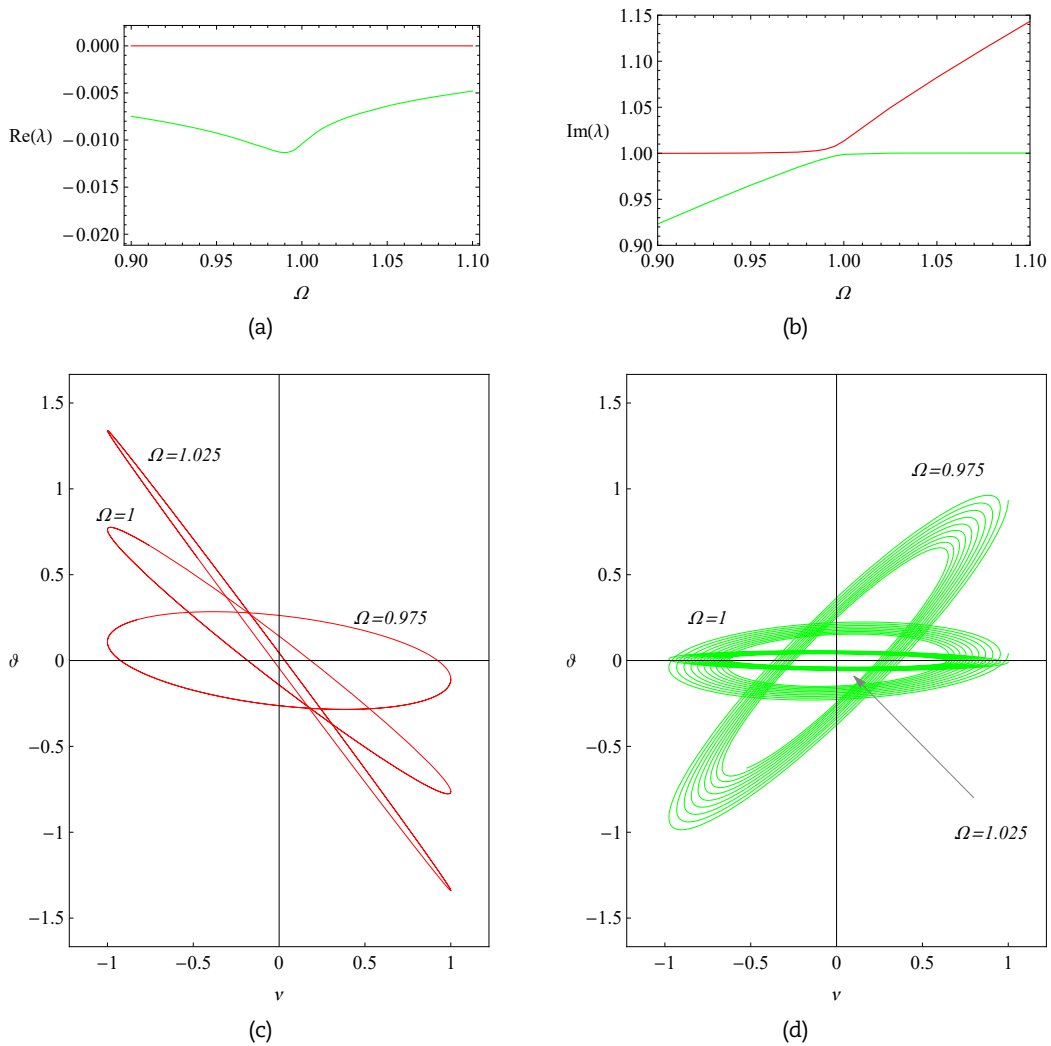


Figure 12. System eigenvalues in the resonant region: (a) real and (b) imaginary part of eigenvalues; (c) critical and (d) stable trajectories in the  $(v, \vartheta)$  plane for three different  $\Omega$  values around the resonance. Critical modes (red lines), stable modes (green lines).

[7] Pagnini, L., Freda, A., Piccardo, G., Uncertainties in the evaluation of one degree-of-freedom galloping onset, *European Journal of Environmental and Civil Engineering*, 2017, 21(7-8), 1043–1063.

[8] Paidoussis, M., Price, S., de Langre, E., *Fluid-structure Interactions - Cross-Flow Induced Instabilities*, Cambridge Univ. Press, 2011.

[9] Nigol, O., Buchan, P., Conductor galloping. II: Torsional mechanism, *IEEE Transactions on Power Apparatus and Systems*, 1981, PAS-100(2), 708–720.

[10] Wu, L., Zuo, D., Numerical evaluation of coupled galloping of slender towers in boundary-layer winds based on a nonlinear analytical model, *Journal of Fluids and Structures*, 2018, 83, 358–371.

[11] Ferretti, M., Zulli, D., Luongo, A., A continuum approach to the nonlinear in-plane galloping of shallow flexible cables, *Advances in Mathematical Physics*, 2019, 2019, 6865730.

[12] Slater, J., Aeroelastic instability of a structural angle section, Ph.D. thesis, The University of British Columbia, Vancouver, Canada, 1969.

[13] Blevins, R., Iwan, W., The galloping response of a two-degree-of-freedom system, *Journal of Applied Mechanics, ASME*, 1974, 41, 1113–1118.

[14] Desai, Y., Shah, A., Popplewell, N., Galloping analysis for two-degree-of-freedom oscillator, *Journal of Engineering Mechanics, ASCE*, 1990, 116(12), 2583–2602.

[15] Yu, P., Shah, A., Popplewell, N., Inertially coupled galloping of iced conductors, *Journal of Applied Mechanics, Transactions of the ASME*, 1992, 59, 140–145.

[16] Yu, P., Popplewell, N., Shah, A., Instability trends of inertially coupled galloping, part I: Initiation, *Journal of Sound and Vibration*, 1995, 183(4), 663–678.

[17] Yu, P., Popplewell, N., Shah, A., Instability trends of inertially coupled galloping, part II: Periodic vibrations, *Journal of Sound and Vibration*, 1995, 183(4), 679–691.



- [18] Jones, K., Coupled vertical and horizontal galloping, *Journal of Engineering Mechanics*, 1992, 118(1), 92–107.
- [19] Liang, S., Li, Q., Li, G., Qu, W., An evaluation of onset wind velocity for 2-D coupled galloping oscillations of tower buildings, *Journal of Wind Engineering and Industrial Aerodynamics*, 1993, 50, 329–340.
- [20] Caracoglia, L., Influence of weather conditions and eccentric aerodynamic loading on the large amplitude aeroelastic vibration of tubular highway poles, *Engineering Structures*, 2007, 29(12), 3550–3566.
- [21] Luongo, A., Piccardo, G., Linear instability mechanisms for coupled translational galloping, *Journal of Sound and Vibration*, 2005, 288(4-5), 1027–1047.
- [22] Piccardo, G., Carassale, L., Freda, A., Critical conditions of galloping for inclined square cylinders, *Journal of Wind Engineering and Industrial Aerodynamics*, 2011, 99(6-7), 748–756.
- [23] Nikitas, N., Macdonald, J., Misconceptions and generalizations of the Den Hartog galloping criterion, *Journal of Engineering Mechanics*, ASCE, 2014, 140(4), 04013005.
- [24] Piccardo, G., A methodology for the study of coupled aeroelastic phenomena, *Journal of Wind Engineering and Industrial Aerodynamics*, 1993, 48, 241–252.
- [25] Yu, P., Desai, Y.M., Shah, A.H., Popplewell, N., Three-degree-of-freedom model for galloping. part I: Formulation, *Journal of Engineering Mechanics*, 1993, 119(12), 2404–2425.
- [26] Gjelstrup, H., Georgakis, C., A quasi-steady 3 degree-of-freedom model for the determination of the onset of bluff body galloping instability, *Journal of Fluids and Structures*, 2011, 27(7), 1021–1034.
- [27] Lou, W., Yang, L., Huang, M., Yang, X., Two-parameter bifurcation and stability analysis for nonlinear galloping of iced transmission lines, *Journal of Engineering Mechanics ASCE*, 2014, 140(11), 04014081.
- [28] He, M., Macdonald, J., An analytical solution for the galloping stability of a 3 degree-of-freedom system based on quasi-steady theory, *Journal of Fluids and Structures*, 2016, 60, 23–36.
- [29] He, M., Macdonald, J., Aeroelastic stability of a 3DOF system based on quasi-steady theory with reference to inertial coupling, *Journal of Wind Engineering and Industrial Aerodynamics*, 2017, 171, 319–329.
- [30] Lou, W., Wu, D., Xu, H., Yu, J., Galloping stability criterion for 3-DOF coupled motion of an ice-accreted conductor, *Journal of Structural Engineering*, ASCE, 2020, 146(5), 0402007.
- [31] Luongo, A., Paolone, A., Perturbation methods for bifurcation analysis from multiple nonresonant complex eigenvalues, *Nonlinear Dynamics*, 1997, 14(3), 193–210.
- [32] Gattulli, V., Di Fabio, F., Luongo, A., Simple and double Hopf bifurcations in aeroelastic oscillators with tuned mass dampers, *Journal of the Franklin Institute*, 2001, 338(2-3), 187–201.
- [33] Luongo, A., Paolone, A., Di Egidio, A., Multiple timescales analysis for 1:2 and 1:3 resonant Hopf bifurcations, *Nonlinear Dynamics*, 2003, 34(3-4), 269–291.
- [34] Gattulli, V., Di Fabio, F., Luongo, A., One to one resonant double Hopf bifurcation in aeroelastic oscillators with tuned mass dampers, *Journal of Sound and Vibration*, 2003, 262(2), 201–217.
- [35] Luongo, A., Di Egidio, A., Paolone, A., Multiscale analysis of defective multiple-Hopf bifurcations, *Computers and Structures*, 2004, 82(31-32), 2705–2722.
- [36] Seyranian, A., Mailybaev, A., *Multiparameter Stability Theory with Mechanical Applications*, World Scientific, Singapore, 2003.
- [37] Luongo, A., Ferretti, M., Can a semi-simple eigenvalue admit fractional sensitivities?, *Applied Mathematics and Computation*, 2015, 255, 165–178.
- [38] Piccardo, G., Tubino, F., Luongo, A., A shear-shear torsional beam model for nonlinear aeroelastic analysis of tower buildings, *Zeitschrift für Angewandte Mathematik und Physik*, 2015, 66(4), 1895–1913.
- [39] Piccardo, G., Tubino, F., Luongo, A., Equivalent nonlinear beam model for the 3-D analysis of shear-type buildings: Application to aeroelastic instability, *International Journal of Non-Linear Mechanics*, 2016, 80, 52–65.
- [40] D’Annibale, F., Ferretti, M., Luongo, A., Shear-shear-torsional homogenous beam models for nonlinear periodic beam-like structures, *Engineering Structures*, 2019, 184, 115–133.
- [41] Piccardo, G., Tubino, F., Luongo, A., Equivalent Timoshenko linear beam model for the static and dynamic analysis of tower buildings, *Applied Mathematical Modelling*, 2019, 71, 77–95.
- [42] Ferretti, M., D’Annibale, F., Luongo, A., Modeling beam-like planar structures by a one-dimensional continuum: an analytical-numerical method, *J. Appl. Comput. Mech.*, 2020, xx(x), 11–24.
- [43] Pagnini, L., Piccardo, G., Solari, G., VIV regimes and simplified solutions by the spectral model description, *Journal of Wind Engineering and Industrial Aerodynamics*, 2020, 198, 104100.
- [44] Perkins, N., Mote Jr., C., Comments on curve veering in eigenvalue problems, *Journal of Sound and Vibration*, 1986, 106(3), 451–463.
- [45] Chen, X., Kareem, A., Curve veering of eigenvalue loci of bridges with aeroelastic effects, *Journal of Engineering Mechanics ASCE*, 2003, 129(2), 146–159.



**ORCID iD**

Angelo Luongo  <https://orcid.org/0000-0003-1426-7825>  
 Francesca Pancella  <https://orcid.org/0000-0002-0894-0078>  
 Giuseppe Piccardo  <https://orcid.org/0000-0002-8983-8138>



© 2021 by the authors. Licensee SCU, Ahvaz, Iran. This article is an open access article distributed under the terms and conditions of the Creative Commons Attribution-NonCommercial 4.0 International (CC BY-NC 4.0 license) (<http://creativecommons.org/licenses/by-nc/4.0/>)

How to cite this article: Angelo Luongo, Francesca Pancella, Giuseppe Piccardo. Flexural-Torsional Galloping of Prismatic Structures with Double-Symmetric Cross-Section, J. Appl. Comput. Mech., 7(SI), 2021, 1049-1069. <https://doi.org/10.22055/JACM.2020.35199.2594>

**Appendix A: Coefficients of the exact equations (13), (21)**

The coefficients appearing in Eq (13) are:

$$\begin{aligned}
 p_1(\Omega) &:= -\alpha_{yy}\alpha_{\vartheta\vartheta}(\Omega) \\
 p_2(\Omega) &:= -\alpha_{yy}^3\alpha_{\vartheta\vartheta}(\Omega) + \alpha_{yy}^2(\alpha_{y\vartheta}\alpha_{\vartheta y} - \alpha_{\vartheta\vartheta}^2(\Omega)) + \alpha_{\vartheta y}\alpha_{\vartheta\vartheta}(\Omega)\beta_{y\vartheta} + \alpha_{yy}[-\alpha_{\vartheta y}\beta_{y\vartheta} + \alpha_{\vartheta\vartheta}(\Omega)(2 + \alpha_{y\vartheta}\alpha_{\vartheta y} - 2\beta_{\vartheta\vartheta})] \\
 p_3(\Omega) &:= -(\alpha_{\vartheta\vartheta}(\Omega) - \alpha_{\vartheta y}\beta_{y\vartheta})[\alpha_{yy}^2\alpha_{\vartheta\vartheta}(\Omega) + \alpha_{yy}(1 - \alpha_{y\vartheta}\alpha_{\vartheta y} + \alpha_{\vartheta\vartheta}^2(\Omega)) + \alpha_{\vartheta y}(-\alpha_{y\vartheta}\alpha_{\vartheta\vartheta}(\Omega) + \beta_{y\vartheta})] \\
 &\quad + \beta_{\vartheta\vartheta}\{\alpha_{yy}[2\alpha_{\vartheta\vartheta}(\Omega) - (\alpha_{yy} + \alpha_{\vartheta\vartheta}(\Omega))(-\alpha_{y\vartheta}\alpha_{\vartheta y} + \alpha_{yy}\alpha_{\vartheta\vartheta}(\Omega))] + \alpha_{\vartheta y}\beta_{y\vartheta}(-\alpha_{yy} + \alpha_{\vartheta\vartheta}(\Omega))\} \\
 &\quad - \alpha_{yy}\alpha_{\vartheta\vartheta}(\Omega)\beta_{\vartheta\vartheta}^2
 \end{aligned}
 \tag{77}$$

The coefficients in Eq (21) are:

$$\begin{aligned}
 J_0 &:= -2(c_d + c'_l)\eta_y\left((c_d + c'_l)\eta_y - c'_m\frac{R}{b}\eta_\vartheta\right)^2\xi_\vartheta - 8c_dc'_m\eta_y\eta_\vartheta\xi_\vartheta^3 \\
 J_1 &:= 2c'_m\eta_\vartheta\xi_y\left(-\frac{R}{b}\left((c_d + c'_l)\eta_y - c'_m\frac{R}{b}\eta_\vartheta\right)^2 - 4\left(2c_d\eta_y - c'_l\eta_y + c'_m\frac{R}{b}\eta_\vartheta\right)\xi_\vartheta^2\right) \\
 J_2 &:= 2\left((c_d + c'_l)\eta_y\left((c_d + c'_l)\eta_y - c'_m\frac{R}{b}\eta_\vartheta\right)^2 - 4c'_m\eta_\vartheta\left(c_d\eta_y - 2c'_l\eta_y + 2c'_m\frac{R}{b}\eta_\vartheta\right)\xi_\vartheta^2\right)\xi_y^2 \\
 J_3 &:= 2c'_m\eta_\vartheta\xi_y\left(\frac{R}{b}\left((c_d + c'_l)\eta_y - c'_m\frac{R}{b}\eta_\vartheta\right)^2 + 4\left(c'_l\eta_y - c'_m\frac{R}{b}\eta_\vartheta\right)\xi_\vartheta^2\right)
 \end{aligned}
 \tag{78}$$

**Appendix B: Asymptotic solutions to the non-resonant flexural-torsional equation (38)**

Equation (38) is recast to make explicit the dependence on  $\mu$ , i.e.:

$$(\Omega^2 - 1 + \mu^2\check{\beta}_{\vartheta\vartheta})(2\xi_\vartheta\Omega - \mu\check{\alpha}_{\vartheta\vartheta}) + \mu^3\check{\alpha}_{\vartheta y}\check{\beta}_{y\vartheta} = 0
 \tag{79}$$

where the following positions hold:

$$\check{\beta}_{\vartheta\vartheta} := \eta_\vartheta c'_m, \quad \check{\alpha}_{\vartheta\vartheta} := \eta_\vartheta \frac{R}{b} c'_m, \quad \check{\alpha}_{\vartheta y} := \eta_\vartheta c'_m, \quad \check{\beta}_{y\vartheta} := \eta_y c'_l
 \tag{80}$$

When  $\Omega$  is small, by neglecting it with respect to 1, it is:

$$\Omega = \frac{1}{2\xi_\vartheta} \left( \mu\check{\alpha}_{\vartheta\vartheta} + \mu^3 \frac{\check{\alpha}_{\vartheta y}\check{\beta}_{y\vartheta}}{1 - \mu^2\check{\beta}_{\vartheta\vartheta}} \right)
 \tag{81}$$

When use is made of Eqs (80), the first of Eqs (39) is obtained. The curve (81) intersects the  $\mu$ -axis at  $\mu = 0$  and

$\mu = \mu_0 := \sqrt{\frac{\check{\alpha}_{\vartheta\vartheta}}{\check{\alpha}_{\vartheta\vartheta}\check{\beta}_{\vartheta\vartheta} - \check{\alpha}_{\vartheta y}\check{\beta}_{y\vartheta}}}$ , which is larger than zero in the hypotheses assumed.

When  $\Omega$  is large, Eq (79) is approximated by:

$$2\xi_\vartheta\left(\frac{\Omega}{\mu}\right)^3 - \check{\alpha}_{\vartheta\vartheta}\left(\frac{\Omega}{\mu}\right)^2 + \check{\alpha}_{\vartheta y}\check{\beta}_{y\vartheta} = 0
 \tag{82}$$

which shows that  $\Omega$  is proportional to  $\mu$ . By solving it by successive approximations:

$$\frac{\Omega}{\mu} \simeq \frac{1}{2\xi_\vartheta} \left( \check{\alpha}_{\vartheta\vartheta} + \frac{\check{\alpha}_{\vartheta y}\check{\beta}_{y\vartheta}}{\left(\frac{\check{\alpha}_{\vartheta\vartheta}}{2\xi_\vartheta}\right)^2} \right)
 \tag{83}$$

from which the second of Eqs (39) is obtained.



### Appendix C: Asymptotic critical eigenvectors close to the resonance

From the eigenvalue problem (45), the normalized eigenvector  $(a_1, a_2)^T = (1, a_2)^T$  is evaluated, in which:

$$a_2 = -\frac{\alpha_{yy} + 2\lambda_1}{\alpha_{y\vartheta} - i\beta_{y\vartheta}} \quad (84)$$

On the stability boundary,  $\lambda_1 = i\omega_1^\pm$ , as given by Eqs (49) and (55). After elementary algebraic manipulations, separating real and imaginary parts, it follows:

$$\begin{aligned} \operatorname{Re} \left( a_2^\pm \right) &= -\frac{\alpha_{yy}\alpha_{y\vartheta} - 2\omega_1^\pm\beta_{y\vartheta}}{\alpha_{y\vartheta}^2 + \beta_{y\vartheta}^2} \\ \operatorname{Im} \left( a_2^\pm \right) &= -\frac{2\omega_1^\pm\alpha_{y\vartheta} + \alpha_{yy}\beta_{y\vartheta}}{\alpha_{y\vartheta}^2 + \beta_{y\vartheta}^2} \end{aligned} \quad (85)$$

